

Decoding drivers of carbon flux attenuation in the oceanic biological pump

<https://doi.org/10.1038/s41586-024-07850-x>

Received: 20 April 2022

Accepted: 18 July 2024

Published online: 11 September 2024

Open access

 Check for updates

M. Bressac^{1,2✉}, E. C. Laurenceau-Cornec^{2,5}, F. Kennedy², A. E. Santoro³, N. L. Paul³, N. Briggs⁴, F. Carvalho⁴ & P. W. Boyd²

The biological pump supplies carbon to the oceans' interior, driving long-term carbon sequestration and providing energy for deep-sea ecosystems^{1,2}. Its efficiency is set by transformations of newly formed particles in the euphotic zone, followed by vertical flux attenuation via mesopelagic processes³. Depth attenuation of the particulate organic carbon (POC) flux is modulated by multiple processes involving zooplankton and/or microbes^{4,5}. Nevertheless, it continues to be mainly parameterized using an empirically derived relationship, the 'Martin curve'⁶. The derived power-law exponent is the standard metric used to compare flux attenuation patterns across oceanic provinces^{7,8}. Here we present in situ experimental findings from C-RESPIRE⁹, a dual particle interceptor and incubator deployed at multiple mesopelagic depths, measuring microbially mediated POC flux attenuation. We find that across six contrasting oceanic regimes, representing a 30-fold range in POC flux, degradation by particle-attached microbes comprised 7–29 per cent of flux attenuation, implying a more influential role for zooplankton in flux attenuation. Microbial remineralization, normalized to POC flux, ranged by 20-fold across sites and depths, with the lowest rates at high POC fluxes. Vertical trends, of up to threefold changes, were linked to strong temperature gradients at low-latitude sites. In contrast, temperature played a lesser role at mid- and high-latitude sites, where vertical trends may be set jointly by particle biochemistry, fragmentation and microbial ecophysiology. This deconstruction of the Martin curve reveals the underpinning mechanisms that drive microbially mediated POC flux attenuation across oceanic provinces.

The biological carbon pump annually supplies 5–10 Gt of carbon (C) to the oceans' interior^{1,2}, driving long-term sequestration and providing energy for deep-sea ecosystems. The pump efficiency is set initially by myriad transformations of newly formed particles in the euphotic zone (including aggregation and grazing), followed by pronounced vertical flux attenuation via mesopelagic processes that ultimately influence atmospheric carbon dioxide (CO₂) concentrations³. The vertical particulate organic carbon (POC) flux attenuation is typically measured by multiple-depth radionuclide sampling, sediment-trap deployments and/or optical particle measurements. They provide estimates of POC flux attenuation often expressed as a power-law exponent or *b* value⁶. The *b* value is widely used to intercompare and understand flux attenuation patterns across different provinces^{7,8,10}. It is also used to explore the role of factors including oxygen¹¹, temperature⁷, primary productivity¹² or floristics^{8,10} in driving global patterns of POC flux attenuation.

Despite over three decades of research, there is no consensus on the controls of POC flux attenuation; opposing latitudinal trends in *b* values have emerged from global syntheses^{8,10}, observations⁷ and model analyses^{13,14} (Extended Data Table 1). Such disagreement is unsurprising as POC flux attenuation is the cumulative signature of distinct

transformations from zooplankton flux-feeding to particle-attached microbial degradation¹⁵. A better understanding of the factors that control the biological carbon pump therefore requires a separation of the processes that jointly set POC flux attenuation. Teasing these roles apart can provide insights (here, directly for microbes and indirectly for zooplankton) into their relative magnitude, vertical trends, controls and degree of influence in setting regional patterns in particle flux attenuation. Such a mechanistic approach will improve model projections^{16,17} needed to resolve the contribution of microbes and zooplankton to current and projected future changes in the functioning of the biological carbon pump^{3,18}.

Particle degradation by attached bacteria, and other microbes (viruses, archaea and microbial eukaryotes including microzooplankton), is pivotal in POC flux attenuation through colonization and transformation of sinking particles^{17,19} (Extended Data Fig. 1). Wide-ranging terms, including particle remineralization, recycling, solubilization and respiration are employed for this microbial degradation process (Extended Data Fig. 1). Here we use microbial remineralization (MR) throughout to represent the microbially mediated component of POC flux attenuation. We present the mesopelagic MR of sinking

¹Sorbonne Université, CNRS, Laboratoire d'Océanographie de Villefranche, Villefranche-sur-Mer, France. ²Institute for Marine and Antarctic Studies, University of Tasmania, Hobart, Tasmania, Australia. ³Department of Ecology, Evolution and Marine Biology, University of California, Santa Barbara, CA, USA. ⁴National Oceanography Centre, European Way, Southampton, UK. ⁵Present address: Univ. Brest, IUEM, CNRS, LEMAR, IRD, Ifremer, Plouzané, France. ✉e-mail: matthieu.bressac@imev-mer.fr

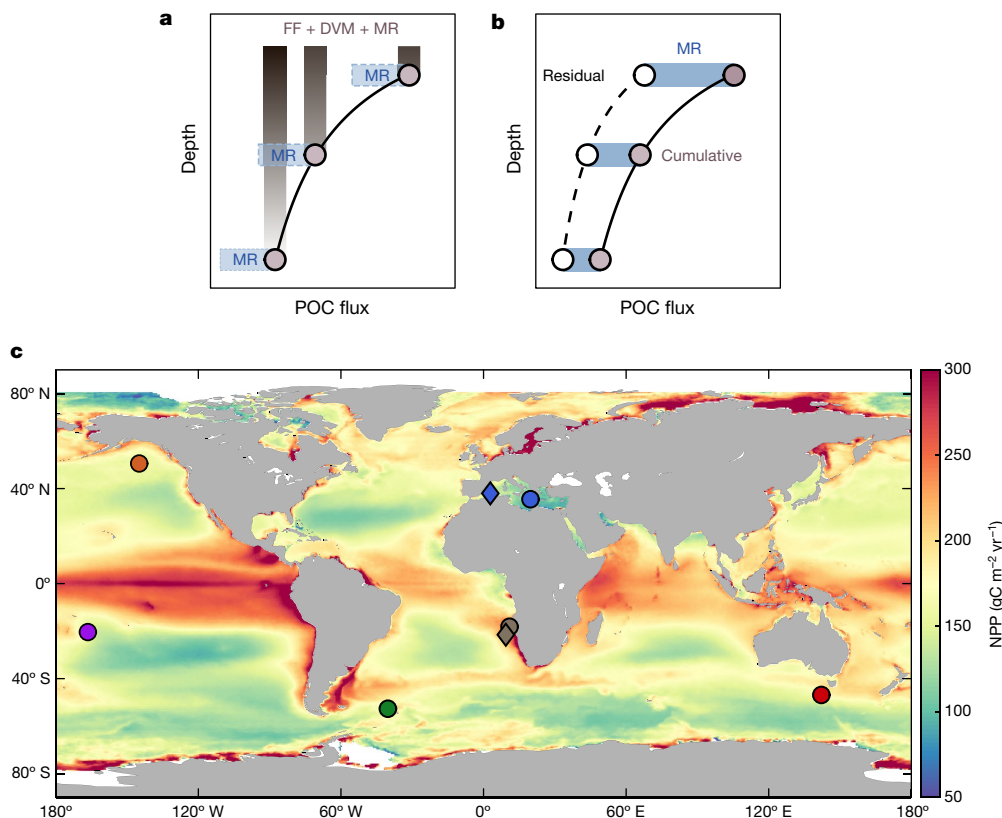


Fig. 1 | Mesopelagic transformations of downward POC flux at multiple depths investigated across contrasting regions. a, Schematic of the cumulative transformations of settling particles (denoted by solid vertical bars) due to zooplankton flux-feeding (FF), DVM and MR before particle interception by C-RESPIRE during the initial collection phase at each of three depths (Extended Data Fig. 2). MR (in blue) represents the subsequent incubation phase of C-RESPIRE in which only MR acts on the intercepted particles to decrease POC. **b**, Deconstruction of the main drivers of the POC flux attenuation. MR (blue areas) is as described in **a** and is inferred from measured O₂ consumption and a fixed RQ (Methods). Dissolved organic C accumulation rates during incubation were low (representing on average 21 ± 16% of MR; Extended Data Table 4), supporting a close coupling between solubilization and MR. The residual POC flux (open circles) corresponds to the (intercepted) POC measured at the end of the multi-day in situ incubation. Cumulative POC flux (filled circles) is reconstructed using the sum of the residual POC and MR (that is, residual POC flux + MR) and should reflect a Martin curve, represented by the solid black line (Methods). **c**, Locations of C-RESPIRE deployments overlaid on a map of satellite-derived net primary productivity (NPP) climatology (2003–2018) (obtained from the NASA Ocean Color website and the CAFE algorithm). Green, SG; brown, BEN; red, SAZ; orange, PAPA; blue, MED; purple, SPSG.

microbially colonized particles, derived from in situ experiments using the C-RESPIRE (that is, Carbon RESPIRE rather than TM-RESPIRE²⁰) dual particle interceptor and incubator⁹ (Extended Data Fig. 2) to explore controls on MR magnitude with depth and across regions, along with its percentage contribution to flux attenuation in the upper mesopelagic (that is, approximately 100–300 m depth), where POC flux is highly attenuated¹.

Deconstructing the Martin curve

The drivers of the Martin curve were decoded by assessing the contribution of MR to POC flux attenuation. The fate of particles intercepted by C-RESPIRE differs fundamentally from sediment traps. Conventionally, with traps, sinking POC is attenuated by MR, zooplankton flux-feeding and diel vertical migration (DVM) until particles are intercepted (Fig. 1a) and instantly preserved. This method, over multiple depths, enables estimation of *b* values but offers few insights into the relative importance of MR, flux-feeding or DVM in setting *b*. In contrast, C-RESPIRE intercepts settling particles that have undergone the joint influence of these processes in overlying waters, then incubates them (Fig. 1a). Particle interception arrests the settling particles (see later) but their capture is required to obtain enough particles to measure MR. Such interception, in situ, is less intrusive than previous

attempts to collect, subsample and/or isolate particles from the sinking assemblage to assess the importance of MR in lab-based^{21,22} and in situ²³ experiments. C-RESPIRE isolates particles within minutes from zooplankton-mediated transformations (Extended Data Fig. 2), and thus in a subsequent multi-day incubation provides only particle transformations driven by MR, based on optode-based microbial respiration rates and a mesopelagic respiratory quotient (RQ; see Methods for caveats). By also measuring POC not transformed by microbes during the incubation (termed the residual POC flux), C-RESPIRE indirectly estimates the cumulative POC flux (that is, MR + residual POC flux), like that measured in sediment traps (Fig. 1b). This residual flux also yields indirect insights into the relative importance of zooplankton-mediated processes (that is, zooplankton were excluded from C-RESPIRE by design) in particle flux attenuation (that is, flux-feeding + DVM).

C-RESPIRES were deployed across regions from highly productive (South Georgia (SG) and Benguela (BEN)) to low-productivity, high nutrient–low chlorophyll (HNLC; Subantarctic Zone (SAZ) and northeast subarctic Pacific (PAPA)) and oligotrophic (Mediterranean (MED) and South Pacific Subtropical Gyre (SPSG)) regimes (Fig. 1c). Some regions had different mesopelagic temperatures, O₂ concentrations (Extended Data Table 2) and phytoplankton assemblages (Extended Data Table 3). These environmental characteristics have been identified by others as potential drivers of mesopelagic POC flux attenuation

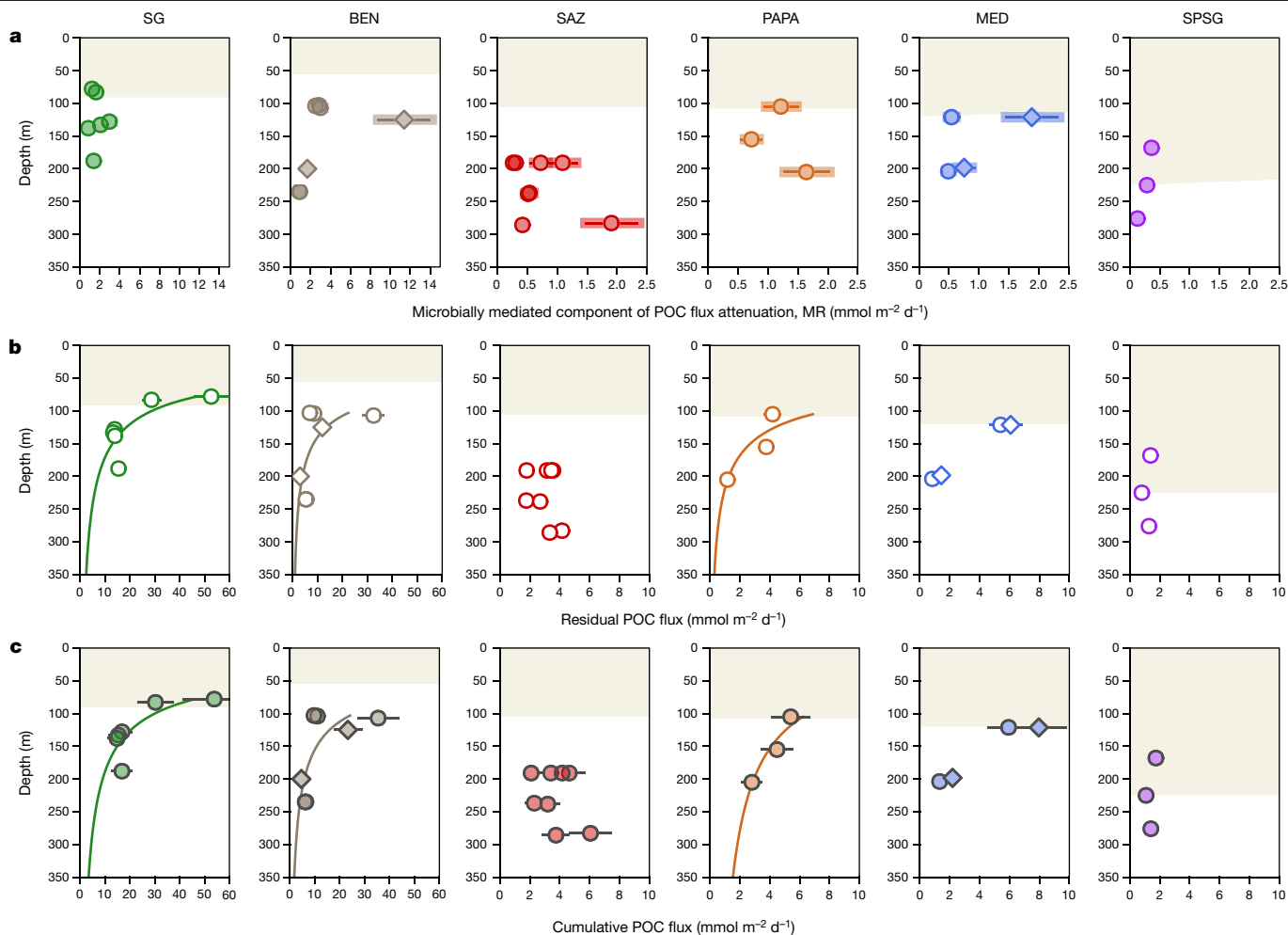


Fig. 2 | Deconstructing POC flux attenuation. **a–c**, Microbially mediated component of the POC flux attenuation, MR (**a**), the residual POC flux (**b**) and the cumulative POC flux (**c**) as a function of depth at the six study sites investigated (same colour code as for Fig. 1c). Note the different flux scales for SG and BEN and for all sites in **a**. Owing to ship logistics, incubation times varied by threefold between sites (Extended Data Table 2). The coloured curves correspond to the best fit of a power-law model (not fitted for MED and SPSG where only two depths below the PPZ were sampled), and error bars were derived using uncertainty-propagation laws (Methods). These Martin curves are presented

(Extended Data Table 1). The diversity of both productivity regimes and phytoplankton assemblages reflects a 30-fold range in POC flux (Fig. 2c). Over the approximately 200-m depth range sampled, cumulative POC flux followed the canonical Martin curve at 5 of the 6 sites (POC flux increased with depth at SAZ). SAZ has a ‘composite’ water column, a HNLC subpolar layer overlying subtropical mesopelagic waters, which may explain the anomalous pattern²⁴. The cumulative POC fluxes reconstructed from C-RESPIRE are Martin curves (Fig. 2c) comparable to those measured using sediment traps⁶, providing confidence in the validity of our reconstruction approach.

The next step in deconstructing the Martin curve is to intercompare vertical trends in MR with the residual POC flux. To do so, we assume constant sinking velocities over the approximately 200-m depth range sampled (Methods). At most sites, there is no evidence of a Martin-type relationship for MR (Fig. 2a), and across all sites the C requirement of particle-attached microbes should readily be met as the median contribution of MR to the cumulative POC flux attenuation ranges from 7% to 29% (Methods), and importantly never exceeds 35% regardless of using bounds of 0.89–0.50 for RQs for unmodified to heavily modified particles (Fig. 2 caption and Extended Data Fig. 3a). Although this trend in MR

only to demonstrate that the cumulative POC flux approach reproduces a power-law attenuation trend. A fixed RQ of 0.70 (that is, for plankton-based particles such as marine snow⁴⁵) was used to calculate MR. The coloured-shaded rectangles in **a** represent the range of values of MR obtained based on the upper (that is, 0.89 for phytoplankton cells⁴⁴) and lower (that is, 0.50 for methane oxidation within particles, the theoretical minimum for RQ⁴⁶) bounds of the range of RQ values used in the sensitivity analysis (Methods). The beige-shaded areas represent the PPZ where new particles are produced.

is consistent with the conclusions from lab-based and field studies^{21–23,25}, such wide-ranging MRs, across six provinces, has not been previously observed. Within our sites, the magnitude of MR changed little with depth. Thus, even though C-RESPIRE halts particle sinking (Extended Data Fig. 2) to conduct multi-day incubations (during which particles, if not intercepted, could sink a further approximately 100–200 m), C-RESPIRE provides a representative estimate of MR across the upper mesopelagic (Methods). In contrast, this MR contribution ranged four-fold across provinces, probably reflecting regionally different patterns in particle flux composition and planktonic assemblages⁴ (see later).

The residual POC flux, probably representing POC inaccessible to microbes, follows a power-law decrease at most sites and dominates the cumulative flux ($80 \pm 13\%$); thus, it largely reflects trends for cumulative POC flux attenuation (Fig. 2b). As flux-feeding and DVM are the other main drivers of particle flux attenuation, vertical trends in the residual POC flux are probably driven by zooplankton-mediated processes in waters overlying each C-RESPIRE (Fig. 1a), assuming that particle-attached microbes within C-RESPIRE had remineralized all available POC by the end of multi-day incubations (Extended Data Fig. 1 and Methods). The Martin-like shape of the residual POC flux

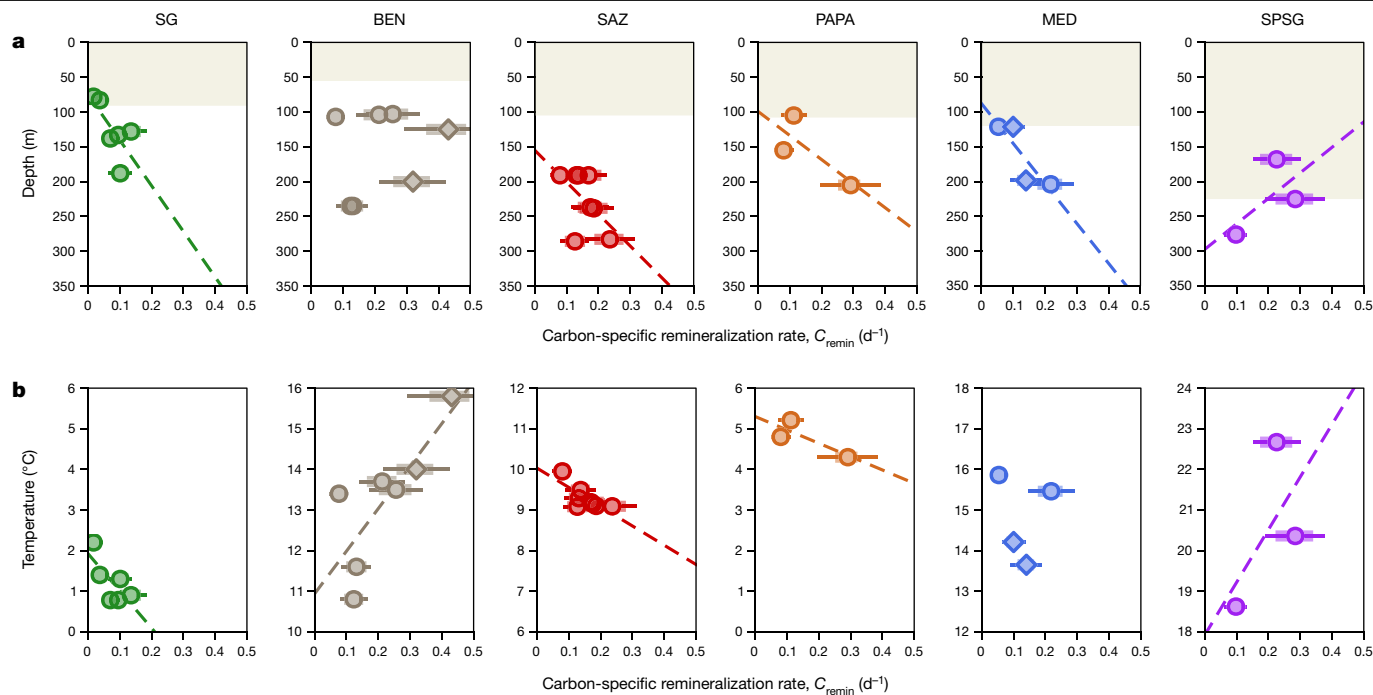


Fig. 3 | Site-specific patterns of C-specific MR. MR was normalized to the cumulative POC flux and incubation time. **a, b**, C_{remin} as a function of depth (**a**) and ambient temperature (**b**)³¹ at each study site shown in Fig. 1c. The median C_{remin} rate ranged from 0.08 d⁻¹ (SG) to 0.23 d⁻¹ (SPSG). The metric C_{remin} enables inspection of the expected relationship (based on Fig. 2) between MR-mediated and cumulative POC fluxes—an increase in C_{remin} with depth (Extended Data

Fig. 4). The coloured-shaded rectangles represent the range of values of C_{remin} obtained based on the upper and lower bounds of the range of RQ values used in the sensitivity analysis, as presented in Fig. 2. The beige-shaded areas in **a** represent the PPZ, as presented in Fig. 2. The dashed lines represent the best fit of the linear model. Error bars were derived using uncertainty-propagation laws (Methods).

probably derives from pronounced vertical distributions of resident²⁶ and vertically migrating^{27,28} flux-feeders in the epipelagic that modulate particle transformations. In summary, the different-shaped profiles of MR-mediated (approximately constant), residual and cumulative POC fluxes (power-law decreases; Fig. 2) indicates that the relative influence of MR on the cumulative POC flux will increase with depth assuming constant sinking velocities (Extended Data Fig. 4).

Patterns in C-specific remineralization

To explore changes in the influence of MR on POC flux attenuation (Fig. 2), we normalized MR to incubation time and cumulative POC flux (Methods). The derived C-specific remineralization rate (C_{remin}) ranged from 0.02 d⁻¹ to 0.43 d⁻¹ across sites and depths (Fig. 3a). The upper bound (0.43 d⁻¹) is several-fold higher than that in previous studies^{21,23}, which subsampled the settling particle assemblage. Our range, when reformulated as C_{remin} , demonstrates that the particle flux supplied enough C (Extended Data Fig. 1 caption) to sustain particle-attached microbial needs in the upper mesopelagic, an unresolved issue highlighted previously^{4,29} (but see ref. 30). This 20-fold range in C_{remin} may be controlled by both site-specific and depth-dependent factors. Comparison of C_{remin} across sites reveals no clear relationship with the magnitude of cumulative POC flux (based on the shallowest C-RESPIRE). Such a relationship is probably confounded by differing biogeochemical characteristics across the sites including: depth of the primary production zone (PPZ); proportion of large diatoms; lability of particles (spring bloom (SG) versus highly transformed (SPSG)); biogenic (SAZ) versus lithogenic (MED); and resulting seasonality of particle properties. These multi-faceted characteristics preclude robust statistical analysis, for example, large diatoms contributed to the setting POC flux at SG (Extended Data Table 3) where high fluxes were little attenuated by microbes (Fig. 2). In contrast, changes in C_{remin} with depth reveal more distinct trends.

Vertical trends in C_{remin} differ between regions (Fig. 3a). At SG, SAZ, PAPA and MED, C_{remin} increased with depth, as expected (Extended Data Fig. 4) considering the approximately constant MR-mediated versus decreasing cumulative POC fluxes (Fig. 2). However, decreasing C_{remin} with depth was observed at sites with larger vertical temperature gradients (BEN ($R^2 = 0.29$) and SPSG ($R^2 = 0.43$)). When plotted against temperature³¹ (Fig. 3b), depth-dependent C_{remin} patterns generally become more conspicuous, suggesting a demarcation in these distinctive trends at sites with vertical gradients of more than 2 °C ($R^2 = 0.80$ and $R^2 = 0.39$ at BEN and SPSG, respectively).

Modes of control on C_{remin}

Mesopelagic temperatures may influence the marked transition in the C_{remin} versus depth relationship between sites (Fig. 3). Temperature is a key driver of microbial community composition³², metabolic activity³³ and organic matter decomposition^{34,35}. The latter two properties are reflected by thermal performance curves (that is, growth or respiration versus temperature^{36–38}) of isolates of marine microbes. Temperature has been proposed as the driver of particle flux attenuation in the palaeo-oceanographic³⁹ and contemporary⁷ oceans. Temperature may control C_{remin} at subtropical sites (BEN and SPSG; Fig. 3b) with pronounced mesopelagic gradients (Extended Data Fig. 5). A similar C_{remin} pattern was reported at Bermuda (subtropical Atlantic), using a C-RESPIRE prototype⁴⁰. This raises the question of whether temperature also exerts control on C_{remin} at mid- and high-latitude sites where MR is relatively invariant with depth (excluding outliers at BEN and MED; Fig. 2a) and C_{remin} increases (Fig. 3).

Mid- and high-latitude sites have upper mesopelagic gradients of less than 2 °C (Fig. 3b). Although no thermal performance curves exist for mesopelagic microbes (that is, under in situ conditions), this physiology versus temperature relationship^{36–38} helps explore the implications of different temperature gradients on C_{remin} . Each temperature– C_{remin}

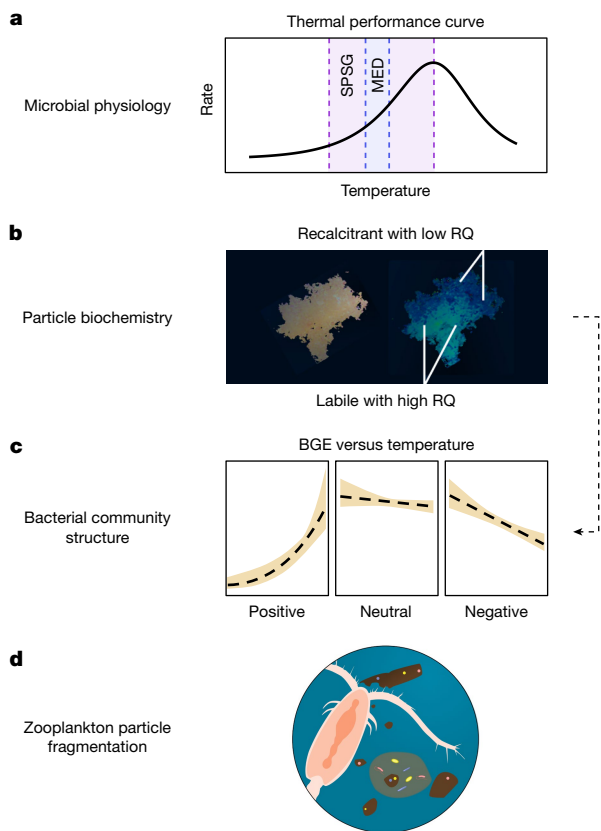


Fig. 4 | Putative evidence for multiple factors controlling distinctive vertical patterns in C_{remin} . **a**, Particle-attached microbial communities may encounter large (SPSG site, purple envelope) versus small (MED site, blue envelope) changes in temperature, as they settle through the water column, differentially altering their physiological performance, as projected by the thermal performance curve relationship, such as in MR. **b**, Sinking particles are characterized by a continuum in biochemical lability (that is, altering substrates) partially controlling the RQ⁴¹. **c**, The thermal sensitivity of soil BGE (analogous to bacterial carbon-use efficiency) is both strain dependent and substrate dependent^{49,50} as represented by the dashed arrow linking **b** and **c**. **d**, In the upper mesopelagic, microzooplankton and mesozooplankton (and also physical disaggregation) fragment large aggregates into smaller slower-sinking particles with large surface area:volume ratios^{55,56} that may promote microbial colonization and enhanced MR.

relationship (Fig. 3b) can be recast using the characteristic shape of a thermal performance curve (Fig. 4a). Although it is not known where on a curve these temperature– C_{remin} data would lie, a marked change in C_{remin} with temperature (straddling slope and plateau) is more likely for a 5 °C gradient than a less than 2 °C gradient (Fig. 4a). Thus, at mid- and high-latitude sites, the influence of temperature on C_{remin} may be diminished, enabling additional factors to set depth-dependent patterns in C_{remin} . Next, we examine the regional characteristics at these mid- and high-latitude sites that may define the functioning of their biological carbon pumps.

Drivers of microbial remineralization

To explore the reasons for the two distinct trends in C_{remin} (Fig. 3), there is insufficient knowledge of the drivers of MR based on the current parameterization of marine models of MR¹⁷. We draw on advances from soil microbiology (joint role of bacterial strain and biochemical substrate on physiology), marine pelagic physiology (thermal performance curves) and mesopelagic microbial ecology (altered community structure with depth) to explore potential explanations.

At higher-latitude sites with small temperature gradients, depth-dependent increases in C_{remin} (Fig. 3) may be disproportionately influenced by vertical gradients in particle characteristics (for example, substrate availability), ecological shifts (community) and/or physiological changes (exo-enzymes to match substrate changes) of particle-attached microbes⁴¹. For example, the joint and complex influence of temperature and substrate on marine bacterial physiological performance is long established^{42,43}. There is indirect evidence of depth-dependent changes in RQ based on a comparison of quotients from unmodified directly sinking phytoplankton cells (RQ = 0.89 (ref. 44)), marine snow (RQ = 0.70 (ref. 45)) to heavily modified particles (RQ = 0.50 (ref. 46)) that suggest that the number of particle transformations as they sink results in altered particle substrate quality with depth (Fig. 4b).

Microbial soil studies show that enzymatic decomposition of biochemically recalcitrant organic matter requires high activation energy, and is more sensitive to changes in temperature than decomposition of more labile organic matter^{47,48}. Soil microbiology studies suggest that the thermal sensitivity of the bacterial growth efficiency (BGE; analogous to carbon-use efficiency) is both substrate dependent⁴⁹ (Fig. 4b) and strain dependent^{49,50} (Fig. 4c). For soil microbes, across multiple substrate and strain permutations^{49,50}, there are combinations in which the BGE versus temperature relationship is positive, that is, BGE decreases (for example, respiration increases more than growth) at lower temperatures. If this relationship holds for oceanic regions, this would increase MR with depth (Fig. 4c). These scenarios are consistent with increasing C_{remin} with depth at some higher-latitude sites (Fig. 3b) and offer the most compelling explanation currently available. In addition to the likelihood of depth dependency of substrate quality⁴¹, there is evidence of changes in microbial community structure and function with depth^{50,51} that together could provide such substrate and strain combinations^{49,50} leading to a constancy in MR (Fig. 2a) in contrast to the power-law decrease in cumulative POC flux, and hence higher C_{remin} at depth (Fig. 4c).

Potential linkages between depth-dependent changes in substrates and microbial community composition are evident from recent mesopelagic studies. Pronounced mesopelagic physico-chemical gradients influence particle-attached microbes and are linked to changes in the composition and function of microbes in the mesopelagic^{51,52}. Others have shown that microscale community ecology of particle-attached bacteria can partially control carbon turnover rates^{53,54}. Bacterial community structure and function (and hence BGEs) may also be influenced by depth-dependent changes in particle characteristics, including sinking rates and surface area:volume ratios driven by mesopelagic particle fragmentation⁵⁵. Fragmentation has been linked to the concept of microbial gardening by microzooplankton⁵⁶ and mesozooplankton⁵⁷ with the exposure of fragmented ‘fresh’ surfaces enabling microbial colonization and potential changes to MR (Fig. 4d). In the absence of a dominant driver such as temperature, at higher-latitude sites (Fig. 3b), we suggest that the most likely additional processes to influence increases in C_{remin} are microbial community structure and function and their interplay with substrates, and potentially the small changes in temperature.

Our main finding of distinct trends in C_{remin} versus depth (increasing versus decreasing), across sites representing wide-ranging environmental, planktonic assemblages and productivity regimes (Fig. 1c), differs from studies proposing temperature as the dominant driver of POC flux attenuation (that is, by MR, flux-feeding and DVM; Fig. 1a) globally^{7,39} (Extended Data Table 1). A previous study³⁹ predominately used sediment cores from low-latitude sites, probably influencing their conclusion on the role of temperature on POC flux attenuation. In another study⁷, sites were either high latitude or low latitude with no intermediates, and can be clustered into high- versus low-latitude trends such that at high latitudes there is no relationship between b values and temperature (their Fig. 2a). Thus, their findings⁷ may not differ markedly from our two distinct trends. Globally, there is a high/mid- to

low-latitude transition from small to large mesopelagic temperature gradients (Extended Data Fig. 5)—as reported here—with regions characterized by small temperature gradients comprising two-thirds of the ocean. Model projections suggest that these mesopelagic trends are unlikely to change in the future^{58,59}, pointing to the continued importance of factors other than temperature in driving POC flux attenuation across mid- and high-latitude regions.

Conclusions

Our study reveals that when POC supply (intercepted sinking particles) and MR (oxygen optode time series and an RQ) are measured concurrently, there is a surfeit of C to sustain the needs of particle-attached microbes. The contribution of MR to the cumulative POC flux attenuation in the upper mesopelagic is less than 30% at all sites, indicative of a lesser but albeit influential role. This trend is consistent with the relative invariance of MR versus depth profiles, which differ from the Martin curve for cumulative POC fluxes. The dominant influence of zooplankton in shaping this curve, that we infer from indirect evidence, probably derives from the strong epipelagic influence of flux-feeders in modulating particle transformations^{55,57}. However, MR may increase in relative importance as an attenuation pathway with depth due to the flat shape of the MR profile relative to that of the rapidly attenuating Martin curve^{26,60}.

Temperature may set C_{remin} but only at low-latitude sites with high vertical temperature gradients, precluding the use of a global relationship to parameterize microbially mediated POC flux attenuation. At higher-latitude sites, multiple causality is likely and there may be important lessons from soil microbiology on concepts such as BGE that link microbial ecology and particle biochemistry, and from lab-based particle experimental approaches⁶¹. This deconstruction of the Martin curve reveals a diverse range of regional biological carbon pumps across the ocean in which microbes have differing influences. This diversity requires more complex representation of POC flux attenuation in biogeochemical models that demarcate the roles of zooplankton flux-feeders and particle-attached microbes. This decoding of the biological carbon pump will provide avenues of enquiry for microbial modellers and experimentalists.

Online content

Any methods, additional references, Nature Portfolio reporting summaries, source data, extended data, supplementary information, acknowledgements, peer review information; details of author contributions and competing interests; and statements of data and code availability are available at <https://doi.org/10.1038/s41586-024-07850-x>.

- Boyd, P. W. & Trull, T. W. Understanding the export of biogenic particles in oceanic waters: is there consensus? *Progr. Oceanogr.* **72**, 276–312 (2007).
- Henson, S. A. et al. A reduced estimate of the strength of the ocean's biological carbon pump. *Geophys. Res. Lett.* **38**, L04606 (2011).
- Kwon, E. Y., Primeau, F. & Sarmiento, J. L. The impact of remineralization depth on the air-sea carbon balance. *Nat. Geosci.* **2**, 630–635 (2009).
- Steinberg, D. K. et al. Bacterial vs. zooplankton control of sinking particle flux in the ocean's twilight zone. *Limnol. Oceanogr.* **53**, 1327–1338 (2008).
- Giering, S. L. et al. Reconciliation of the carbon budget in the ocean's twilight zone. *Nature* **507**, 480–483 (2014).
- Martin, J. H., Knauer, G. A., Karl, D. M. & Broenkow, W. W. VERTEX: carbon cycling in the northeast Pacific. *Deep Sea Res.* **34**, 267–285 (1987).
- Marsay, C. M. et al. Attenuation of sinking particulate organic carbon flux through the mesopelagic ocean. *Proc. Natl Acad. Sci. USA* **112**, 1089–1094 (2015).
- Guidi, L. et al. A new look at ocean carbon remineralization for estimating deepwater sequestration. *Glob. Biogeochem. Cycles* **29**, 1044–1059 (2015).
- Boyd, P. W., McDonnell, A., Valdez, J., LeFevre, D. & Gall, M. P. RESPIRE: an in situ particle interceptor to conduct particle remineralization and microbial dynamics studies in the oceans' twilight zone. *Limnol. Oceanogr. Methods* **13**, 494–508 (2015).
- Henson, S. A., Sanders, R. & Madsen, E. Global patterns in efficiency of particulate organic carbon export and transfer to the deep ocean. *Glob. Biogeochem. Cycles* **26**, GB1028 (2012).
- Pavia, F. J. et al. Shallow particulate organic carbon regeneration in the South Pacific Ocean. *Proc. Natl Acad. Sci. USA* **116**, 9753–9758 (2019).
- Lutz, M. J., Caldeira, K., Dunbar, R. B. & Behrenfeld, M. J. Seasonal rhythms of net primary production and particulate organic carbon flux to depth describe the efficiency of biological pump in the global ocean. *J. Geophys. Res. Oceans* **112**, C10011 (2007).
- Weber, T., Cram, J. A., Leung, S. W., DeVries, T. & Deutsch, C. Deep ocean nutrients imply large latitudinal variation in particle transfer efficiency. *Proc. Natl Acad. Sci. USA* **113**, 8606–8611 (2016).
- Cram, J. A. et al. The role of particle size, ballast, temperature, and oxygen in the sinking flux to the deep sea. *Glob. Biogeochem. Cycles* **32**, 858–876 (2018).
- Buesseler, K. O. & Boyd, P. W. Shedding light on processes that control particle export and flux attenuation in the twilight zone of the open ocean. *Limnol. Oceanogr.* **54**, 1210–1232 (2009).
- Ormand, M. M., Govindarajan, R., He, J. & Mahadevan, A. Sinking flux of particulate organic matter in the oceans: sensitivity to particle characteristics. *Sci. Rep.* **10**, 5582 (2020).
- Nguyen, T. T. et al. Microbes contribute to setting the ocean carbon flux by altering the fate of sinking particulates. *Nat. Commun.* **13**, 1657 (2022).
- Henson, S. A. et al. Uncertain response of ocean biological carbon export in a changing world. *Nat. Geosci.* **15**, 248–254 (2022).
- Leu, A. O., Eppley, J. M., Burger, A. & DeLong, E. F. Diverse genomic traits differentiate sinking-particle-associated versus free-living microbes throughout the oligotrophic open ocean water column. *mBio* **13**, e01569-22 (2022).
- Bressac, M. et al. Resupply of mesopelagic dissolved iron controlled by particulate iron composition. *Nat. Geosci.* **12**, 995–1000 (2019).
- Collins, J. R. et al. The multiple fates of sinking particles in the North Atlantic Ocean. *Glob. Biogeochem. Cycles* **29**, 1471–1494 (2015).
- Belcher, A. et al. Depth-resolved particle-associated microbial respiration in the northeast Atlantic. *Biogeochemistry* **13**, 4927–4943 (2016).
- Karl, D. M., Knauer, G. A. & Martin, J. H. Downward flux of particulate organic matter in the ocean: a particle decomposition paradox. *Nature* **332**, 438–441 (1988).
- Herrera-Borreguero, L. & Rintoul, S. R. Regional circulation and its impact on upper ocean variability south of Tasmania. *Deep Sea Res.* **58**, 2071–2081 (2011).
- Iversen, M. H. Carbon export in the ocean: a biologist's perspective. *Ann. Rev. Mar. Sci.* **15**, 357–381 (2023).
- Stukel, M. R., Ohman, M. D., Kelly, T. B. & Biard, T. The roles of suspension-feeding and flux-feeding zooplankton as gatekeepers of particle flux into the mesopelagic ocean in the Northeast Pacific. *Front. Mar. Sci.* **6**, 397 (2019).
- Goldblatt, R. H., Mackas, D. L. & Lewis, A. G. Mesozooplankton community characteristics in the NE subarctic Pacific. *Deep Sea Res.* **46**, 2619–2644 (1999).
- Steinberg, D. K., Cope, J. S., Wilson, S. E. & Kobari, T. A comparison of mesopelagic mesozooplankton community structure in the subtropical and subarctic North Pacific Ocean. *Deep Sea Res.* **55**, 1615–1635 (2008).
- Burd, A. B. et al. Assessing the apparent imbalance between geochemical and biochemical indicators of meso- and bathypelagic biological activity: what the @ \$#! is wrong with present calculations of carbon budgets? *Deep Sea Res.* **57**, 1557–1571 (2010).
- Herdnd, G. J. & Reinthaler, T. Microbial control of the dark end of the biological pump. *Nat. Geosci.* **6**, 718–724 (2013).
- Brewer, P. G. & Peltzer, E. T. Depth perception: the need to report ocean biogeochemical rates as functions of temperature, not depth. *Phil. Trans. R. Soc. A* **375**, 20160319 (2017).
- Kong, L. F. et al. Illuminating key microbial players and metabolic processes involved in the remineralization of particulate organic carbon in the ocean's twilight zone by metaproteomics. *Appl. Environ. Microbiol.* **87**, e00986–21 (2021).
- Vazquez-Dominguez, E., Vaque, D. & Gasol, J. M. Ocean warming enhances respiration and carbon demand of coastal microbial plankton. *Glob. Change Biol.* **13**, 1327–1334 (2007).
- Iversen, M. H. & Ploug, H. Temperature effects on carbon-specific respiration rate and sinking velocity of diatom aggregates—potential implications for deep ocean export processes. *Biogeochemistry* **10**, 4073–4085 (2013).
- Cavan, E. L. & Boyd, P. W. Effect of anthropogenic warming on microbial respiration and particulate organic carbon export rates in the sub-Antarctic Southern Ocean. *Aquat. Microb. Ecol.* **82**, 111–127 (2018).
- Apple, J. K., Del Giorgio, P. A. & Kemp, W. M. Temperature regulation of bacterial production, respiration, and growth efficiency in a temperate salt-marsh estuary. *Aquat. Microb. Ecol.* **43**, 243–254 (2006).
- Yung, C. M. et al. Thermally adaptive tradeoffs in closely related marine bacterial strains. *Environ. Microbiol.* **17**, 2421–2429 (2015).
- Boscolo-Galazzo, F., Crichton, K. A., Barker, S. & Pearson, P. N. Temperature dependency of metabolic rates in the upper ocean: a positive feedback to global climate change? *Glob. Planet. Change* **170**, 201–212 (2018).
- Boscolo-Galazzo, F. et al. Temperature controls carbon cycling and biological evolution in the ocean twilight zone. *Science* **371**, 1148–1152 (2021).
- McDonnell, A. M. P., Boyd, P. W. & Buesseler, K. O. Effects of sinking velocities and microbial respiration rates on the attenuation of particulate carbon fluxes through the mesopelagic zone. *Glob. Biogeochem. Cycles* **29**, 175–193 (2015).
- Boyd, P. W. & Kennedy, F. Microbes in a sea of sinking particles. *Nat. Microbiol.* **6**, 1479–1480 (2021).
- Pomeroy, L. R. & Wiebe, W. J. Temperature and substrates as interactive limiting factors for marine heterotrophic bacteria. *Aquat. Microb. Ecol.* **23**, 187–204 (2001).
- López-Urrutia, Á. & Morán, X. A. G. Resource limitation of bacterial production distorts the temperature dependence of oceanic carbon cycling. *Ecology* **88**, 817–822 (2007).
- Williams, P. J., le, B. & Robertson, J. E. Overall plankton oxygen and carbon dioxide metabolism: the problem of reconciling observations and calculations of photosynthetic quotients. *J. Plankton Res.* **13**, 153–169 (1991).
- Tanioka, T. & Matsumoto, K. Stability of marine organic matter respiration stoichiometry. *Geophys. Res. Lett.* **47**, e2019GL085564 (2020).
- del Giorgio, P. A. & Williams, P. J. (eds) *Respiration in Aquatic Ecosystems* (Oxford Univ. Press, 2005).

47. Fierer, N., Craine, J. M., McLauchlan, K. & Schimel, J. P. Litter quality and the temperature sensitivity of decomposition. *Ecology* **86**, 320–326 (2005).
48. Craine, J. M., Fierer, N. & McLauchlan, K. K. Widespread coupling between the rate and temperature sensitivity of organic matter decay. *Nat. Geosci.* **3**, 854–857 (2010).
49. Pold, G. et al. Carbon use efficiency and its temperature sensitivity covary in soil bacteria. *mBio* **11**, e02293–19 (2020).
50. Smith, T. P., Clegg, T., Bell, T. & Pawar, S. Systematic variation in the temperature dependence of bacterial carbon use efficiency. *Ecol. Lett.* **24**, 2123–2133 (2021).
51. DeLong, E. F. et al. Community genomics among stratified microbial assemblages in the ocean's interior. *Science* **311**, 496–503 (2006).
52. Baumas, C. M. et al. Mesopelagic microbial carbon production correlates with diversity across different marine particle fractions. *ISME J.* **15**, 1695–1708 (2021).
53. Datta, M. S., Sliwerska, E., Gore, J., Polz, M. F. & Cordero, O. X. Microbial interactions lead to rapid micro-scale successions on model marine particles. *Nat. Commun.* **7**, 11965 (2016).
54. Enke, T. N., Leventhal, G. E., Metzger, M., Saavedra, J. T. & Cordero, O. X. Microscale ecology regulates particulate organic matter turnover in model marine microbial communities. *Nat. Commun.* **9**, 2743 (2018).
55. Briggs, N., Dall'Olmo, G. & Claustre, H. Major role of particle fragmentation in regulating biological sequestration of CO₂ by the oceans. *Science* **367**, 791–793 (2020).
56. Poulsen, L. K., Moldrup, M., Berge, T. & Hansen, P. J. Feeding on copepod fecal pellets: a new trophic role of dinoflagellates as detritivores. *Mar. Ecol. Prog. Ser.* **441**, 65–78 (2011).
57. Mayor, D. J., Sanders, R., Giering, S. L. & Anderson, T. R. Microbial gardening in the ocean's twilight zone: detritivorous metazoans benefit from fragmenting, rather than ingesting, sinking detritus. *Bioessays* **36**, 1132–1137 (2014).
58. Bindoff, N. L. et al. Changing ocean, marine ecosystems, and dependent communities. In *IPCC Special Report on the Ocean and Cryosphere in a Changing Climate* (eds Pörtner, H.-O. et al.) 447–587 (Cambridge Univ. Press, 2019).
59. Cooley, S. et al. Oceans and coastal ecosystems and their services. In *Climate Change 2022: Impacts, Adaptation and Vulnerability. Contribution of Working Group II to the Sixth Assessment Report of the Intergovernmental Panel on Climate Change* (eds Pörtner, H.-O. et al.) 379–550 (Cambridge Univ. Press, 2022).
60. Stemmann, L., Jackson, G. A. & Gorsky, G. A vertical model of particle size distributions and fluxes in the midwater column that includes biological and physical processes—Part II: application to a three year survey in the NW Mediterranean Sea. *Deep Sea Res. I* **51**, 885–908 (2004).
61. Alcolombri, U. et al. Sinking enhances the degradation of organic particles by marine bacteria. *Nat. Geosci.* **14**, 775–780 (2021).

Publisher's note Springer Nature remains neutral with regard to jurisdictional claims in published maps and institutional affiliations.



Open Access This article is licensed under a Creative Commons Attribution-NonCommercial-NoDerivatives 4.0 International License, which permits any non-commercial use, sharing, distribution and reproduction in any medium or format, as long as you give appropriate credit to the original author(s) and the source, provide a link to the Creative Commons licence, and indicate if you modified the licensed material. You do not have permission under this licence to share adapted material derived from this article or parts of it. The images or other third party material in this article are included in the article's Creative Commons licence, unless indicated otherwise in a credit line to the material. If material is not included in the article's Creative Commons licence and your intended use is not permitted by statutory regulation or exceeds the permitted use, you will need to obtain permission directly from the copyright holder. To view a copy of this licence, visit <http://creativecommons.org/licenses/by-nc-nd/4.0/>.

© The Author(s) 2024

Methods

Site characteristics

High-productivity regions. Regions downstream of South Georgia (SG) and in the Benguela Current offshore of Namibia (BEN) were sampled using C-RESPIRE within the framework of the UK COMICS (Controls over Ocean Mesopelagic Interior Carbon Storage) project⁶² during research cruises DY086 and DY090 onboard the RSS *Discovery*. At SG (52.7° S, 40.2° W), 6 individual C-RESPIRE incubations to provide measurements of the microbially mediated component of POC flux attenuation (MR) were performed during November to December 2017. These naturally iron-fertilized waters downstream of SG are characterized by an intense phytoplankton bloom dominated by large diatoms⁶³, sustaining high downwards C export fluxes⁶⁴. Relatively low in situ temperatures, ranging from 0.8 °C to 1.8 °C, were observed at the SG site (Extended Data Table 2). In the BEN region, stations BS (21.6° S, 9.4° E) and BN (18.2° S, 11.0° E) were sampled in May to June 2018 to provide 7 individual C-RESPIRE measurements of MR. Intense coastal upwelling occurs in this locale, supplying nutrients that support high pelagic biological productivity and downwards C export. High rates of mesopelagic respiration are responsible for the formation of a subsurface low-oxygen zone⁶⁵. During COMICS 2, intermittent low-oxygen events (25–60 $\mu\text{mol kg}^{-1}$) were observed between about 100-m and 440-m depth, with a persistent low-oxygen band between 300 m and 400 m (ref. 66), and C-RESPIRE incubations were performed at dissolved oxygen concentrations as low as 45 $\mu\text{mol kg}^{-1}$ at 235-m depth at the BN station (Extended Data Table 2).

HNLC regions. The SAZ site (46.9° S, 142.2° E) is located in the Subantarctic Zone southwest of Tasmania. It corresponds to the location of the Australian Southern Ocean Time Series (SOTS) site⁶⁷, a long-term particle flux time-series observatory operating at 1,000-m, 2,000-m and 3,800-m depth⁶⁸. This locale often has both low dissolved silicate and iron concentrations over the annual cycle, along with a phytoplankton community dominated by haptophytes, flagellates and small diatoms⁶⁹. Deployments of C-RESPIRE were performed from the R/V *Investigator* in March (2019), that is, about 2–3 months after the peak of phytoplankton productivity (December) and near the end of the downwards export period. Ocean Station Papa (PAPA) in the northeast subarctic Pacific was sampled during the US EXPORTS NP campaign onboard the R/V *Roger Revelle* in late summer (August to September) 2018^{70,71}. Owing to low dissolved iron supply, this HNLC area is characterized by a modest primary productivity signature (March to April) dominated by diatoms and coccolithophores⁷², that is reflected by low–medium fluxes of the biological carbon pump⁷³. For technical reasons, only data obtained during the last deployment (Epoch 3) of the EXPORTS NP voyage are available.

Oligotrophic regions. MR at two sites within the Mediterranean Sea (MED) were obtained using the C-RESPIRE deployed during the French PEACETIME cruise⁷⁴ (<https://doi.org/10.17600/17000300>) onboard the R/V *Pourquoi Pas?* in May to June 2017. This enclosed basin is characterized by a west-to-east gradient of increasing oligotrophy, and by intense atmospheric deposition of desert dust from the Sahara⁷⁵. C-RESPIRES were deployed in the western Algerian basin (37.9° N, 2.9° E) and Ionian Sea (35.5° N, 19.8° E). The South Pacific Subtropical Gyre (SPSG) is characterized by the most oligotrophic waters of the global ocean⁷⁶. The edge of the gyre (20.4° S, 166.5° W) has a subsurface chlorophyll maxima at about 150-m depth, and was sampled for MR in November 2019 onboard the R/V *L'Atalante* during the TONGA cruise⁷⁷ (<https://doi.org/10.17600/18000884>).

The C-RESPIRE dual particle interceptor and incubator

Principles of operation and sampling microbial communities. The C-RESPIRE particle interceptor and incubator is designed to

non-intrusively intercept sinking particles, concentrate them within a 1.45 l volume of (unpoisoned) filtered seawater, and then incubate them at in situ pressure and temperature (Extended Data Fig. 2). Reference 9 provides a detailed discussion on the potential artefacts associated with the C-RESPIRE method, such as the implications of halting sinking particles, particles sitting on the base plate of the instrument during incubations potentially reducing degradation rates⁶¹, and a demonstration of the minor contribution of free-living bacteria to microbial respiration rates. C-RESPIRE consists of a titanium cylinder with a collection area of 0.0124 m². At its entrance, a baffle limits the turbulence and resuspension of the sinking particles that ultimately settle into an indented rotating sphere (IRS). Pre-programmed rotations (typically every 5–10 min) of the IRS transfer particles into an inner chamber (1.45 l) equipped with an oxygen optode. The IRS ensures the exclusion of mesozooplankton and isolation of the inner chamber when not rotating (Extended Data Fig. 2). The roughly 1- to 3-day particle collection phase (Extended Data Table 2) promotes the accumulation of sinking particles in the chamber, along with their attached microbial consortia, including heterotrophic bacteria and microzooplankton^{78,79}. This accumulation of sinking particles ensures that the remineralization signature most closely corresponds to that of the attached microbial assemblage, as opposed to free-living heterotrophic bacteria potentially present in the <0.2- μm filtered seawater initially used to fill the inner chamber.

Deployment of the free-drifting C-RESPIRE mooring array.

C-RESPIRES were deployed below the PPZ depth (except at the SPSG site where one C-RESPIRE was deployed within the PPZ; Fig. 2), that is, the depth where the in vivo chlorophyll fluorescence drops to 10% of its maximum value⁸⁰. Before deployment, the C-RESPIRES were gently filled with <0.2- μm filtered seawater collected at each deployment depth. A lagged delay in particle interception of about 3 h was pre-programmed to avoid collection of sinking particles above the programmed depth. Two or three C-RESPIRES were deployed on a free-drifting surface-tethered array comprising wave-damping floats and/or 25-m-long bungee cord to reduce the vertical motion of the mooring line. Temperature and pressure sensors (RBR) were used to confirm the deployment depth and assess the vertical motions of the mooring during the deployment. Deployment duration ranged from about 2 days to 5 days and was adapted to weather conditions, ship logistics and other activities onboard.

Sampling procedure and data collection.

Collection (T_{COLL}) and incubation (T_{INCUB}) times were chosen as a function of the deployment duration and the estimated particle flux magnitude in the region at the time of the year of each voyage (Extended Data Table 2). After recovery of the array of two or three C-RESPIRES, seawater above the IRS was siphoned off and the inner chamber was sampled from each C-RESPIRE. Samples were stored in the dark at 4 °C until further processing. These steps were performed within <1 h of recovery of the C-RESPIRES. The absence of mesozooplankton in the inner chamber was confirmed by visual inspection. The 1.45-l sample was split into 8 equal fractions using a custom particle splitter similar to that reported in ref. 81. POC-designated subsamples were filtered through pre-combusted 13-mm- or 25-mm-diameter GF/F or QMA filters, and stored at –20 °C until processing and analysis. POC samples were acidified overnight with 2 M HCl to remove inorganic C, and then dried at 60 °C for 2 days. Samples were then analysed on a CHN analyser (Thermo Finnigan EA 1112 Series Flash Elemental Analyser).

Remineralization rate

Oxygen time series. The inner chamber of each C-RESPIRE was equipped with an oxygen optode (Aanderaa 3830 or 4831 series). Dissolved oxygen concentrations were corrected for pressure, salinity and temperature according to the Aanderaa Operating Manual

and ref. 82. Optodes were post-calibrated at the Mediterranean Institute of Oceanography (Marseille, France) or deployed on a CTD (conductivity, temperature and depth) instrument to cross-compare with dissolved oxygen concentrations obtained with the Winkler method (O_2 range = 230–330 $\mu\text{mol kg}^{-1}$, slope = 0.94 ± 0.01 , $R^2 = 0.98$, $P < 0.001$). The total amount of dissolved oxygen consumed during incubation (ΔO_2 , mmolO_2) was obtained by using the equation:

$$\Delta O_2 = (O_{2 \text{ PRE-INCUB}} - O_{2 \text{ POST-INCUB}}) \times 1.45$$

where $O_{2 \text{ PRE-INCUB}}$ and $O_{2 \text{ POST-INCUB}}$ are dissolved oxygen concentrations ($\text{mmolO}_2 \text{ l}^{-1}$) measured at the start and end of the incubation, respectively, and 1.45 is the volume of the inner chamber (l). Care was taken to attain dissolved oxygen concentrations close to ambient concentrations before the start of the incubation phase. However, it is noted that owing to the strong variability in dissolved oxygen concentrations in the Benguela area⁶⁶, for two C-RESPIRE measurements, pre-incubation dissolved oxygen concentrations diverge by more than 15% from ambient dissolved oxygen concentrations before the incubation with CTD cast(s) (BN31 deployment; Extended Data Table 2).

Respiratory quotient. A respiratory quotient ($\text{RQ} = \Delta \text{DIC} / -\Delta O_2$, where DIC is dissolved inorganic carbon) is used to convert an oxygen-based to a carbon-based remineralization rate (see below). RQ varies depending on the stoichiometry and oxidation state of the substrate, and the metabolic pathway used⁸³. As a consequence, a large range of RQs has been reported from incubations and field measurements⁸⁴. Assuming complete oxidation, the average composition of phytoplankton cells results in an RQ of 0.89 (ref. 44). The lower bound of RQs is the theoretical minimum of 0.50 for methane oxidation⁴⁶. This range of published values of RQs for different particle types straddle individual phytoplankton cells (that is, no particle transformations) to heavily transformed particles. Within these bounds, ref. 45 reported from two independent methods a global estimate of RQ in the surface ocean of about 0.70 with small spatial variability. Over longer time periods, a $C_{\text{org}}:O_2$ conversion factor of 0.69 (that is, 117/170) representative of the stoichiometric ratio of particle remineralization has been obtained, for the mesopelagic realm deeper than 400 m, across the South Atlantic, Indian and Pacific basin⁸⁵. These RQ values are broadly representative of plankton-based particles such as marine snow and mesopelagic conditions (that is, differing substrate quality, microbial communities). Consequently, we selected an RQ of 0.70—reported by refs. 45,85 as an interim value—to convert the oxygen-based remineralization rate to C.

In addition, we measured microbially mediated RQ values during the SOLACE voyage (Southern Ocean Large Area Carbon Export; 4 December 2020 to 15 January 2021) at three study sites straddling an approximately 9 °C mesopelagic temperature range: one subantarctic site (SAZ), and two sites south of the Polar Front (PF1 and PF2; Extended Data Table 5). At these sites, surface-tethered particle interceptor traps (PITs) were deployed for 3 days at 3 depths between about 180 m and 280 m. PIT tubes containing no preservative were used for intercepting ‘fresh’ sinking particles. After recovery of the PITs, tubes were transferred to a temperature-control lab (set to ambient mixed-layer surface ocean temperature at each site). The overlying waters were gently siphoned off and particles were collected from each tube and were immediately placed in 4-ml glass sample vials (Merck, Z256064), each containing PreSens O_2 (SF-RPSu4) and CO_2 (SF-CD2R) sensors and ambient (filtered) seawater from each depth. Calibration of the sensors was conducted in accordance with the manufacturer’s instructions. The O_2 sensors were standardized using a two-point calibration (0%, 100% saturated air) and the CO_2 sensors were calibrated using a 6-point calibration with specific gas mixes (0%, 0.04%, 0.06%, 0.08%, 1%, 5%; BOC Linde gas). Glass vials containing particles and seawater were placed in individual wells of a 24-well flat-bottom plate (Corning

CLS3527). Each plate contained a total of 16 samples from unpreserved PITs, and 4 negative control vials (filtered seawater collected from the same site and depth). The sample vials were incubated for 12 h at in situ temperature, with readings taken for O_2 and CO_2 concentrations using the VisiSens TD (PreSens). The readings were corrected for site and depth temperature and salinity following the manufacturer’s instructions. Subsequently, all samples were processed for preservation using 0.5% glutaraldehyde for further analysis and microscopy. If zooplankton were found within a sample, that sample was removed from the subsequent analysis, focusing only on mesopelagic microbes. Sample images were processed using PreSens IDL evaluation software. Images obtained over a 12-h period were used to determine particle RQs. The amount of O_2 consumed (molO_2) and CO_2 produced (molCO_2) during incubation was obtained using the following equation:

$$\Delta O_2 = ((O_{2 \text{ PRE-INCUB}} - O_{2 \text{ POST-INCUB}}) - (O_{2 \text{ CONTROL PRE-INCUB}} - O_{2 \text{ CONTROL POST-INCUB}}))$$

$$\Delta CO_2 = ((CO_{2 \text{ PRE-INCUB}} - CO_{2 \text{ POST-INCUB}}) - (CO_{2 \text{ CONTROL PRE-INCUB}} - CO_{2 \text{ CONTROL POST-INCUB}}))$$

At the three sites and depths, the total alkalinity versus salinity relationship was used to calculate the total alkalinity from the Global Ocean Data Analysis Project (GLODAP) hydrographic section data⁸⁶. This dataset was also used to estimate the change in the partial pressure of CO_2 (p_{CO_2}). For each salinity, temperature and p_{CO_2} value at each depth across the three sites, a Matlab routine was used to calculate a Revelle factor (R)—the incremental change in p_{CO_2} divided by the incremental change in DIC, so $R = [\Delta p_{CO_2} / p_{CO_2}] \div [\Delta \text{DIC} / \text{DIC}]$. R was calculated from the total alkalinity values (Salinity), p_{CO_2} comes from a typical value in the field near the site, and DIC is calculated with p_{CO_2} and the total alkalinity in CO2SYS routine (CO2SYSv3 for MATLAB). The values obtained were used to calculate the apparent RQ of each sample vial, as follows:

$$\text{aRQ} = \Delta \text{DIC} / -\Delta O_2$$

At the shallowest depth, aRQ values ranged from 0.77 to 0.88 (Extended Data Table 5), consistent with the RQ values of 0.70 from global analyses^{45,85} and 0.89 for a substrate similar to the average composition of planktonic material⁴⁴. These aRQ values generally decreased with depth but never reached the theoretical minimum of 0.5 (for methane oxidation⁴⁶) except for one outlier at the deepest depth at the PF1 site. The release of DOC during remineralization (Extended Data Table 4) and the potential for subsequent partial oxidation of this DOC pool by microbes (leading to a decrease in O_2 but not a corresponding increase in CO_2 or DIC) could potentially lead to RQs <0.5. These depth-dependent changes in aRQ can be linked to the remineralization of labile particles by microbes and the biochemical sequence of degradation that occurs as particles sink, becoming less labile and more recalcitrant. It is noted that apparent RQs may change depending on incubation time (that is, decrease further during longer incubations; F.K., unpublished data), which may be linked to the solubilization of DOC and its eventual use as a microbial substrate.

RQ sensitivity analysis. To test how the choice of an RQ value will influence the outcome of the results presented in Figs. 2 and 3, we conducted a sensitivity analysis using a range of fixed and depth-varying RQ values. Fixed RQ values were chosen to reflect sinking particles that have been degraded by multiple particle transformations as they settle through the mesopelagic realm: an upper bound of 0.89 (for phytoplankton cells⁴⁴), a mid-point of 0.70 (for plankton-based particles such as marine snow⁴⁵) and a lower bound of 0.50 (that is, the theoretical minimum for methane⁴⁶ formed within marine particles such as faecal pellets⁸⁷).

Article

Depth dependency for RQ was parameterized using our mesopelagic aRQ values measured during the 2020–2021 SOLACE voyage (Extended Data Table 5). To take into account differences in C-RESPIRE sampling depths relative to the base of the PPZ (z_{PPZ}) between sites (Fig. 2 and Extended Data Table 5), sampling depths were standardized to z_{PPZ} . On the basis of the aRQ values measured during SOLACE and assuming an RQ value of 0.89 (ref. 44) at z_{PPZ} (and above), the following relationship was obtained:

$$RQ_z = -0.21 \cdot 10^{-2} \times (z - z_{PPZ}) + 0.89$$

Applying this relationship to our dataset (that is, $z - z_{PPZ}$ between 0 m and 181 m), we obtained a depth-varying RQ (RQ_z where z represents the depth) ranging between 0.51 and 0.89 (Extended Data Fig. 3e) with an average value of 0.73 ± 0.12 . The contribution of MR to the cumulative POC flux attenuation and vertical profiles in C_{remin} obtained using the tested range of fixed and depth-varying RQ values are presented in Extended Data Fig. 3. This sensitivity analysis reveals that the contribution of MR to the cumulative POC flux attenuation (Extended Data Fig. 3a) and the depth-dependent increases in C_{remin} (Extended Data Fig. 3b–e) are largely insensitive to the choice of an RQ, such that the influence of MR never exceeds 35%. This insensitivity is mainly due to the dominance of the residual POC flux over MR at most sites.

Deconstruction of the POC flux

Here we expand on how the POC flux was teased apart into three components: MR, the residual flux ($F_{RESIDUAL}$) and the cumulative flux (F_{CUMUL}). Conceptually, settling particles undergo continuous transformation from attached microbes and discrete transformations by zooplankton¹⁵. Upon interception by C-RESPIRE, particles are predominantly transformed by attached bacteria. However, if these sinking particles had not been halted by the C-RESPIRE, they would have continued to have been modified by both zooplankton and particle-attached microbes. By measuring MR in C-RESPIRE, it is possible to first derive an estimate of the POC that would have been available to zooplankton to transform (termed $F_{RESIDUAL}$) had the particles continued to sink. Next, by combining MR and $F_{RESIDUAL}$ we can estimate F_{CUMUL} . Below we outline both the equations used and also several of the assumptions that have to be made for this deconstruction.

Microbial contribution. The microbially mediated component of the POC flux attenuation (MR, $\text{mmolC m}^{-2} \text{d}^{-1}$), was calculated from ΔO_2 and a fixed RQ of 0.70 (see previous section for justification):

$$MR = \Delta O_2 \times RQ / 0.0124 / T_{COLL}$$

where 0.0124 is the collection area (m^2) and T_{COLL} is the collection time (d) of the C-RESPIRE. We acknowledge that MR (and hence $F_{RESIDUAL}$) is partly dependent on the incubation time, which varied between sites due to ship logistical constraints (Extended Data Table 2). The O_2 consumption rate was typically constant over the first approximately 30–48 h of incubations and then the rate often decreased, indicative of the onset of substrate limitation (Extended Data Fig. 1). Hence, our estimates of MR will probably reflect the contribution of MR to the cumulative POC flux attenuation (that is, MR/F_{CUMUL}) at the deployment depth. However, this interpretation—of the onset of substrate limitation—must be reconciled with the lack of change in MR observed with depth (Fig. 2a); substrate limitation at a shallower depth should result in a decrease in MR at deeper depths unless there is a change in the particle-attached microbial assemblage that results in the utilization of other substrates¹⁹.

On the basis of the assumption that MR becomes substrate limited after more than 30 h of incubation (Extended Data Fig. 1), MR could have

been underestimated (and hence $F_{RESIDUAL}$ slightly overestimated) by about 25% for the 1-day incubations (such as at BEN), but as this underestimation would apply to measurements at each depth the overall trends will not alter. In addition, the dominance of $F_{RESIDUAL}$ over MR at most sites (Fig. 2) means that $F_{RESIDUAL}$ would have been overestimated by a much smaller percentage, and hence this trend would not alter despite the uncertainties regarding shorter incubations in relation to substrate limitation.

Residual POC flux. This flux ($F_{RESIDUAL}$, $\text{mmolC m}^{-2} \text{d}^{-1}$) was obtained using the following equation:

$$F_{RESIDUAL} = [POC]_{POST-INCUB} \times 1.45 / 0.0124 / T_{COLL}$$

where $[POC]_{POST-INCUB}$ is the concentration of POC remaining at the end of the multi-day incubation (mmol l^{-1}) and 1.45 is the volume of the incubation chamber (l). $F_{RESIDUAL}$ is interpreted here as the POC that is not available to the microbes due to the onset of substrate limitation (Extended Data Fig. 1). However, on shorter incubations, such as at BEN, it is possible that a small proportion of this residual POC could be available for particle-attached microbes.

Cumulative POC flux. The cumulative POC flux (F_{CUMUL} , $\text{mmolC m}^{-2} \text{d}^{-1}$) is reconstructed using the sum of $F_{RESIDUAL}$ with MR ($F_{CUMUL} = F_{RESIDUAL} + MR$). F_{CUMUL} is comparable to the flux measured using conventional sediment traps and can be contrasted with published values and/or concomitant sediment-trap measurements. At PAPA, F_{CUMUL} was twofold to threefold higher than POC fluxes simultaneously measured at the same depths⁷¹ (but note, different collection periods and aspect ratio of the traps versus C-RESPIRE, which both influence the magnitude of the POC flux), but within the range of previous measurements at this site^{88,89}. In MED, F_{CUMUL} obtained at 195-m depth was consistent with the range of previous estimates ($0.4\text{--}3.0 \text{ mmol m}^{-2} \text{d}^{-1}$)⁹⁰, but about fourfold higher than fluxes simultaneously measured at 250-m depth using a PPS5 conical sediment trap⁹¹. This discrepancy in flux estimates probably reflects the power-law decrease of the POC flux expected between 195-m and 250-m depth, but also the lower collection efficiency of conical traps compared with cylindrical traps⁹² such as the C-RESPIRE.

POC flux attenuation. The rate of POC flux attenuation (Fig. 2) was obtained using the power-law function or ‘Martin curve’⁶:

$$F_z = F_{z_0} \times (z/z_0)^{-b}$$

where z and z_0 are the depths of the flux, F_{z_0} is the POC flux at the reference depth (the shallowest flux in this study), and b is the attenuation coefficient. The b value is highly sensitive to the choice of the reference depth¹⁵ and the number of data points per profile⁹³, and is usually estimated over the first >500 m of the water column. In this study that focused on the upper mesopelagic and deployed C-RESPIRES within a narrow depth range (about 200 m), the Martin curves presented in Fig. 2 are only informative.

Carbon-specific remineralization rate. The C-specific remineralization rate, C_{remin} (d^{-1}), is calculated using the equation:

$$C_{remin} = \Delta O_2 \times RQ / (\Delta O_2 \times RQ + [POC]_{POST-INCUB} \times 1.45) / T_{INCUB}$$

Relationships between C_{remin} and depth or temperature were assessed via a linear model fit (Fig. 3). Considering the large range of dissolved oxygen concentrations observed at BEN (about $45\text{--}220 \mu\text{mol kg}^{-1}$) and the potential role of oxygen in controlling C_{remin} (refs. 11,84), the relationship between C_{remin} and dissolved oxygen concentration was also assessed. At BEN, a lower correlation was obtained between

C_{remin} and dissolved oxygen concentrations ($R^2 = 0.60$, $P = 0.15$) relative to the correlation between C_{remin} and temperature ($R^2 = 0.80$, $P < 0.01$).

Error propagation. The errors in MR, F_{RESIDUAL} , F_{CUMUL} and C_{remin} were calculated by propagating the uncertainties from subsampling the assemblage of particles collected at the end of the C-RESPIRE incubations using a splitter (that introduces an approximately 10% variability), POC analysis, O_2 measurements and the 20% error from assuming a constant RQ⁸³.

Justification for assuming constant particle sinking rates for the upper mesopelagic

In this study, owing to a lack of published observations of particle sinking rates over the upper mesopelagic, we assume constant sinking speed, implying that the POC loss per day versus POC loss per metre relationship remains unchanged with depth. This assumption allows us to discuss the relative constancy of MR and its relative importance as an attenuation pathway with depth. Changes in sinking velocities with depth (in the water column above each C-RESPIRE) are inherently taken into account for particles intercepted by C-RESPIRES deployed at different depths (Fig. 1a). There is evidence of an increase of the average sinking velocity with depth over the mesopelagic (that is, about 100 m to 1,000 m)^{94,95}. However, the applicability of this trend to the upper mesopelagic (in our study about 100 m to 300 m depth) where aggregation, solubilization and fragmentation can influence sinking velocity in opposing ways (for example, fragmentation slows particle settling⁵⁵) is unknown.

Data availability

The dataset generated during this study will be available after publication (end of embargo 1 October 2024) at <https://doi.org/10.17882/100610>.

62. Sanders, R. J. et al. Controls over Ocean Mesopelagic Interior Carbon Storage (COMICS): fieldwork, synthesis, and modeling efforts. *Front. Mar. Sci.* **3**, 136 (2016).
63. Korb, R. E. et al. Regional and seasonal differences in microplankton biomass, productivity, and structure across the Scotia Sea: implications for the export of biogenic carbon. *Deep Sea Res. II* **59**, 67–77 (2012).
64. Rembauville, M., Manno, C., Tarling, G. A., Blain, S. & Salter, I. Strong contribution of diatom resting spores to deep-sea carbon transfer in naturally iron-fertilized waters downstream of South Georgia. *Deep Sea Res.* **115**, 22–35 (2016).
65. Shannon, L. V. & Nelson, G. in *The South Atlantic Past and Present Circulation* (eds Wefer, G. W. H. et al.) 163–210 (Springer, 1996).
66. Lovecchio, E., Henson, S., Carvalho, F. & Briggs, N. Oxygen variability in the offshore northern Benguela upwelling system from glider data. *J. Geophys. Res. Oceans* **127**, e2022JC019063 (2022).
67. Trull, T. W. et al. Autonomous multi-trophic observations of productivity and export at the Australian Southern Ocean Time Series (SOTS) reveal sequential mechanisms of physical–biological coupling. *Front. Mar. Sci.* **6**, 525 (2019).
68. Wynn-Edwards, et al. Particle fluxes at the Australian Southern Ocean Time Series (SOTS) achieve organic carbon sequestration at rates close to the global median, are dominated by biogenic carbonates, and show no temporal trends over 20-years. *Front. Earth Sci.* **8**, 329 (2020).
69. Eriksen, R. et al. Seasonal succession of phytoplankton community structure from autonomous sampling at the Australian Southern Ocean Time Series (SOTS) observatory. *Mar. Ecol. Progr. Ser.* **589**, 13–31 (2018).
70. Siegel, D. et al. An operational overview of the EXPORT Processes in the Ocean from RemoTe Sensing (EXPORTS) Northeast Pacific field deployment. *Elem. Sci. Anth.* **9**, 00107 (2021).
71. Estapa, M. et al. Biogenic sinking particle fluxes and sediment trap collection efficiency at Ocean Station Papa. *Elementa* **9**, 00122 (2021).
72. Boyd, P. & Harrison, P. J. Phytoplankton dynamics in the NE subarctic Pacific. *Deep Sea Res. II* **46**, 2405–2432 (1999).
73. Buesseler, K. O. et al. High-resolution spatial and temporal measurements of particulate organic carbon flux using thorium-234 in the northeast Pacific Ocean during the EXPORT Processes in the Ocean from RemoTe Sensing field campaign. *Elementa* **8**, 030 (2020).
74. Guieu, C. et al. Introduction: Process studies at the air–sea interface after atmospheric deposition in the Mediterranean Sea—objectives and strategy of the PEACETIME oceanographic campaign (May–June 2017). *Biogeosciences* **17**, 5563–5585 (2020).
75. Guerzoni, S. et al. The role of atmospheric deposition in the biogeochemistry of the Mediterranean Sea. *Progr. Oceanogr.* **44**, 147–190 (1999).

76. Claustre, H., Sciandra, A. & Vault, D. Introduction to the special section bio-optical and biogeochemical conditions in the south east Pacific in late 2004: the BIOSOPE program. *Biogeosciences* **5**, 679–691 (2008).
77. Bonnet, S. et al. Natural iron fertilization by shallow hydrothermal sources fuels diazotroph blooms in the ocean. *Science* **380**, 812–817 (2023).
78. Lampitt, R. S., Wishner, K. F., Turley, C. M. & Angel, M. V. Marine snow studies in the Northeast Atlantic Ocean: distribution, composition and role as a food source for migrating plankton. *Mar. Biol.* **116**, 689–702 (1993).
79. Kiorboe, T. Marine snow microbial communities: scaling of abundances with aggregate size. *Aquat. Microb. Ecol.* **33**, 67–75 (2003).
80. Owens, S. A., Pike, S. & Buesseler, K. O. Thorium-234 as a tracer of particle dynamics and upper ocean export in the Atlantic Ocean. *Deep Sea Res. II* **116**, 42–59 (2015).
81. Lamborg, C. H. et al. The flux of bio- and lithogenic material associated with sinking particles in the mesopelagic “twilight zone” of the northwest and North Central Pacific Ocean. *Deep Sea Res. II* **55**, 1540–1563 (2008).
82. Thierry, V. et al. *Processing Argo Oxygen Data at the DAC Level* Version 2.3.1 (2018).
83. Berggren, M., Lapiere, J. F. & Del Giorgio, P. A. Magnitude and regulation of bacterioplankton respiratory quotient across freshwater environmental gradients. *ISME J.* **6**, 984–993 (2012).
84. Robinson, C. Microbial respiration, the engine of ocean deoxygenation. *Front. Mar. Sci.* **5**, 533 (2019).
85. Anderson, L. A. & Sarmiento, J. L. Redfield ratios of remineralization determined by nutrient data analysis. *Glob. Biogeochem. Cycles* **8**, 65–80 (1994).
86. Lauvset, S. et al. GLODAPv2.2022: the latest version of the global interior ocean biogeochemical data product. *Earth Syst. Sci. Data* **14**, 5543–5572 (2022).
87. Karl, D. M. & Tilbrook, B. D. Production and transport of methane in oceanic particulate organic matter. *Nature* **368**, 732–734 (1994).
88. Boyd, P. W. et al. Transformations of biogenic particulates from the pelagic to the deep ocean realm. *Deep Sea Res. II* **46**, 2761–2792 (1999).
89. Mackinson, B. L., Moran, S. B., Lomas, M. W., Stewart, G. M. & Kelly, R. P. Estimates of micro-, nano-, and picoplankton contributions to particle export in the northeast Pacific. *Biogeosciences* **12**, 3429–3446 (2015).
90. Ramondenc, S. et al. An initial carbon export assessment in the Mediterranean Sea based on drifting sediment traps and the Underwater Vision Profiler data sets. *Deep Sea Res. I* **117**, 107–119 (2016).
91. Bressac, M. et al. Subsurface iron accumulation and rapid aluminum removal in the Mediterranean following African dust deposition. *Biogeosciences* **18**, 6435–6453 (2021).
92. Baker, C. A., Estapa, M. L., Iversen, M., Lampitt, R. & Buesseler, K. Are all sediment traps created equal? An intercomparison study of carbon export methodologies at the PAP-SO site. *Progr. Oceanogr.* **184**, 102317 (2020).
93. Cael, B. B. & Bisson, K. Particle flux parameterizations: quantitative and mechanistic similarities and differences. *Front. Mar. Sci.* **5**, 395 (2018).
94. Berelson, W. M. Particle settling rates increase with depth in the ocean. *Deep Sea Res. II* **49**, 237–251 (2001).
95. Villa-Alfageme, M. et al. Geographical, seasonal, and depth variation in sinking particle speeds in the North Atlantic. *Geophys. Res. Lett.* **43**, 8609–8616 (2016).
96. Boyd, P. W., Ellwood, M. J., Tagliabue, A. & Twining, B. S. Biotic and abiotic retention, recycling and remineralization of metals in the ocean. *Nat. Geosci.* **10**, 167–173 (2017).
97. Kamalanathan, M. et al. Exoenzymes as a signature of microbial response to marine environmental conditions. *mSystems* **5**, e00290–20 (2020).
98. Cezairliyan, B. & Ausubel, F. M. Investment in secreted enzymes during nutrient-limited growth is utility dependent. *Proc. Natl Acad. Sci. USA* **114**, E7796–E7802 (2017).
99. Mahmoudi, N. et al. Illuminating microbial species-specific effects on organic matter remineralization in marine sediments. *Environ. Microbiol.* **22**, 1734–1747 (2020).
100. Smith, E. M. Coherence of microbial respiration rate and cell-specific bacterial activity in a coastal planktonic community. *Aquat. Microb. Ecol.* **16**, 27–35 (1998).
101. Cabré, A., Shields, D., Marinov, I. & Kostadinov, T. S. Phenology of size-partitioned phytoplankton carbon-biomass from ocean color remote sensing and CMIP5 models. *Front. Mar. Sci.* **3**, 39 (2016).

Acknowledgements This dataset results from the efforts of many individuals involved in different international programmes. We thank the captains, crew and all scientists of the R/V *Investigator*, *Pourquoi Pas?*, *L’Atalante*, *RSS Discovery* and *Roger Revelle* for the deployment and recovery of the C-RESPIRES across the six sites; the CSIRO Marine National Facility (MNF) for its support in the form of sea time on RV *Investigator*, support personnel, scientific equipment and data management (all data and samples acquired on the voyage are made publicly available in accordance with MNF policy); C. Young and P. Waller for help in developing a new version of the C-RESPIRE; and L. Bach, L. Legendre and C. Guieu for their comments on the paper. This manuscript has benefited from discussions with members of the SCOR working group 161 ReMO (Respiration in the Mesopelagic Ocean). This study was partly funded by the Australian Research Council by a Laureate awarded to P.W.B. (FL160100131), and by a Marie Skłodowska-Curie Postdoctoral European Fellowship awarded to M.B. (European Union Seventh Framework Programme FP7/2007-2013; agreement no. P10F-GA-2012-626734). F.C. and N.B. were funded by a European Research Council Consolidator Grant (GOCART, agreement no. 724416). South Georgia and Benguela cruises were funded by the Natural Environment Research Council through the COMICS project (Controls over Ocean Mesopelagic Interior Carbon Storage; NE/M020835/1). This study is also a contribution to the PEACETIME project, a joint initiative of the MERMEC and ChArMEc components supported by CNRS-INSU, IFREMER, CEA and Météo-France as part of MISTRALS coordinated by INSU. The TONGA project was funded by the TGIR Flotte Océanographique Française, the A-MiDeX (Aix-Marseille University), the LEFE-CYBER and GMMC programmes and the ANR (ANR-18-CE01-0016). The authors would like to acknowledge support from the National Aeronautics

Article

and Space Administration (NASA) as part of the EXport Processes in the Ocean from RemoTe Sensing (EXPORTS) programme award 80NSSC18K1431.

Author contributions M.B. and P.W.B. designed the study and wrote the paper. M.B. collected the data at SAZ, MED and SPSG; E.C.L.-C. at SG; A.E.S. and N.L.P. at PAPA; N.B. and F.C. at BEN. F.K. collected the RQ dataset and helped interpret the results. All the authors commented on and contributed to the development of the paper.

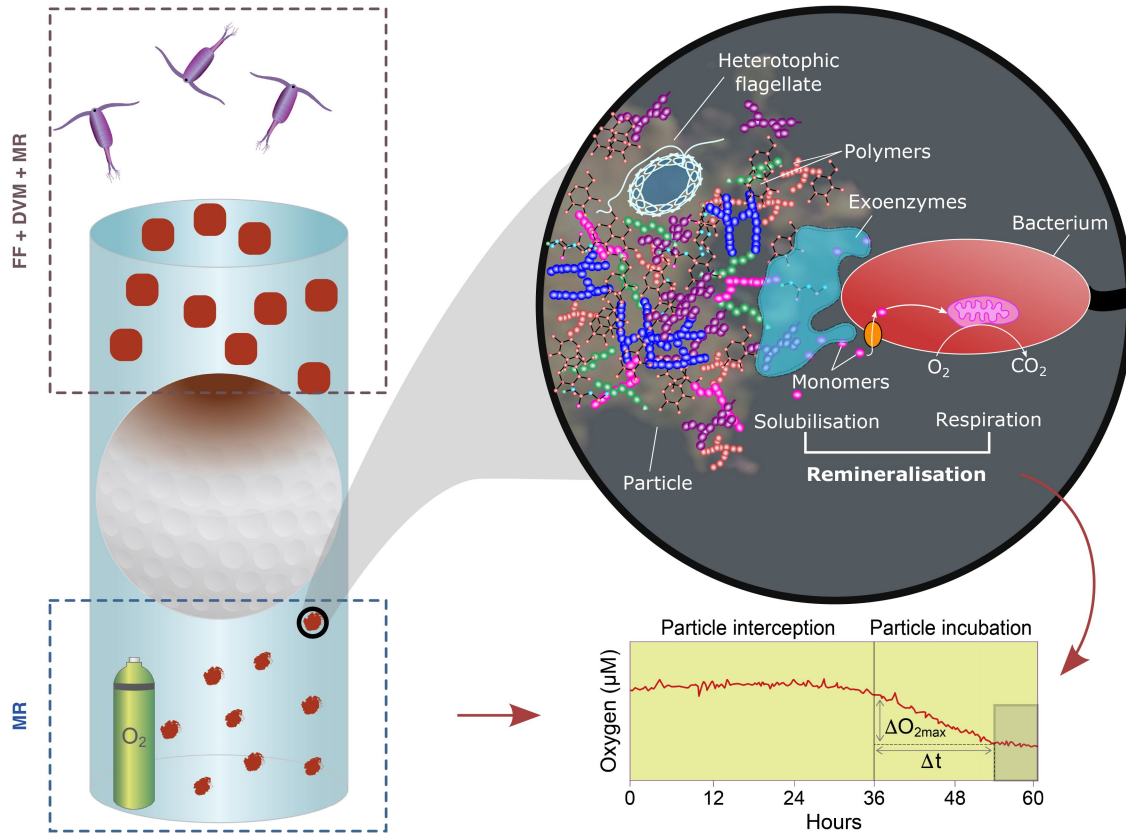
Competing interests The authors declare no competing interests.

Additional information

Correspondence and requests for materials should be addressed to M. Bressac.

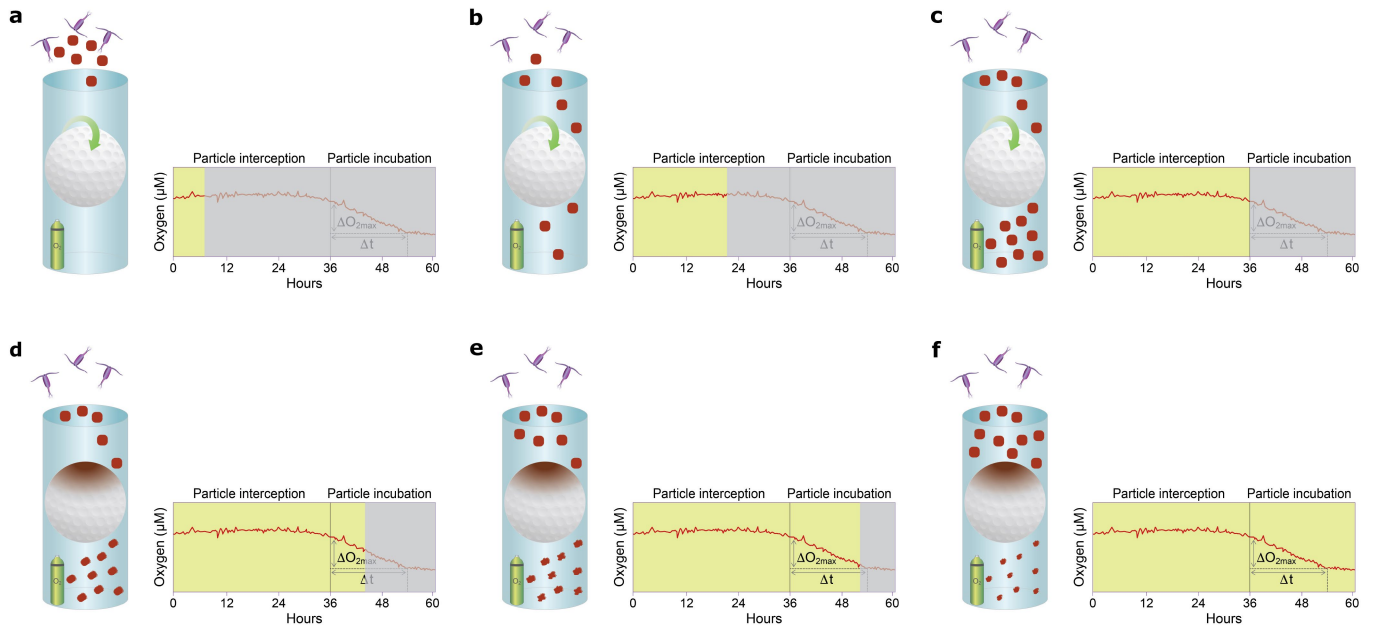
Peer review information *Nature* thanks Clarissa Karthäuser and the other, anonymous, reviewer(s) for their contribution to the peer review of this work.

Reprints and permissions information is available at <http://www.nature.com/reprints>.



Extended Data Fig. 1 | Conceptual linkages between solubilisation, respiration, remineralisation, and microbially-mediated fragmentation of particles intercepted by and incubated within C-RESPIRE and POC flux attenuation. Representation of how C flux attenuation within the inner chamber of C-RESPIRE (left panel) driven by bacterial solubilisation of particles using exo-enzymes is linked to measured bacterially-driven respiration (as a decrease in O_2 (lower right panel) converted to C using a respiratory quotient (see main text)). Other microbes, including heterotrophic microflagellates (upper right panel), contribute to particle fragmentation and degradation⁵⁶ (see also the Supplementary Video 1 from ref. 96). The oxygen optode time-series during the multi-day incubation phase is characterised by a typical decrease in the rate of MR toward the end of the incubation (i.e., after ~24–48 h; grey area on the oxygen time-series) (see also ref. 9), indicative of the onset of substrate limitation for microbes. Kamalanathan et al.⁹⁷ reported a robust

relationship between oceanic POC stocks and C-acquiring exoenzymes that revealed the links between the C needed for bacterial physiology from POC substrates (i.e., polysaccharide depolymerization). This coupling between solubilisation and respiration is further supported by the low accumulation rate of dissolved organic C within the C-RESPIRE inner chamber during incubations (Extended Data Table 4). There is growing evidence of strong links between exoenzyme activity, environmental sensing by attached bacteria^{19,98}, microbial biomass⁹⁷, and C utilisation⁹⁹. Bacterial growth is correlated with respiration¹⁰⁰, and bacterial respiration is the major driver (~90%) of the bacterial carbon demand (total amount of C required to sustain the heterotrophic metabolism, i.e., production plus respiration) based on a compilation of >200 paired bacterial production and respiration from 0–200 m depth from the US-JGOFS open ocean global study⁴³. Hence bacterial respiration closely tracks bacterial carbon demand under natural conditions⁴³.

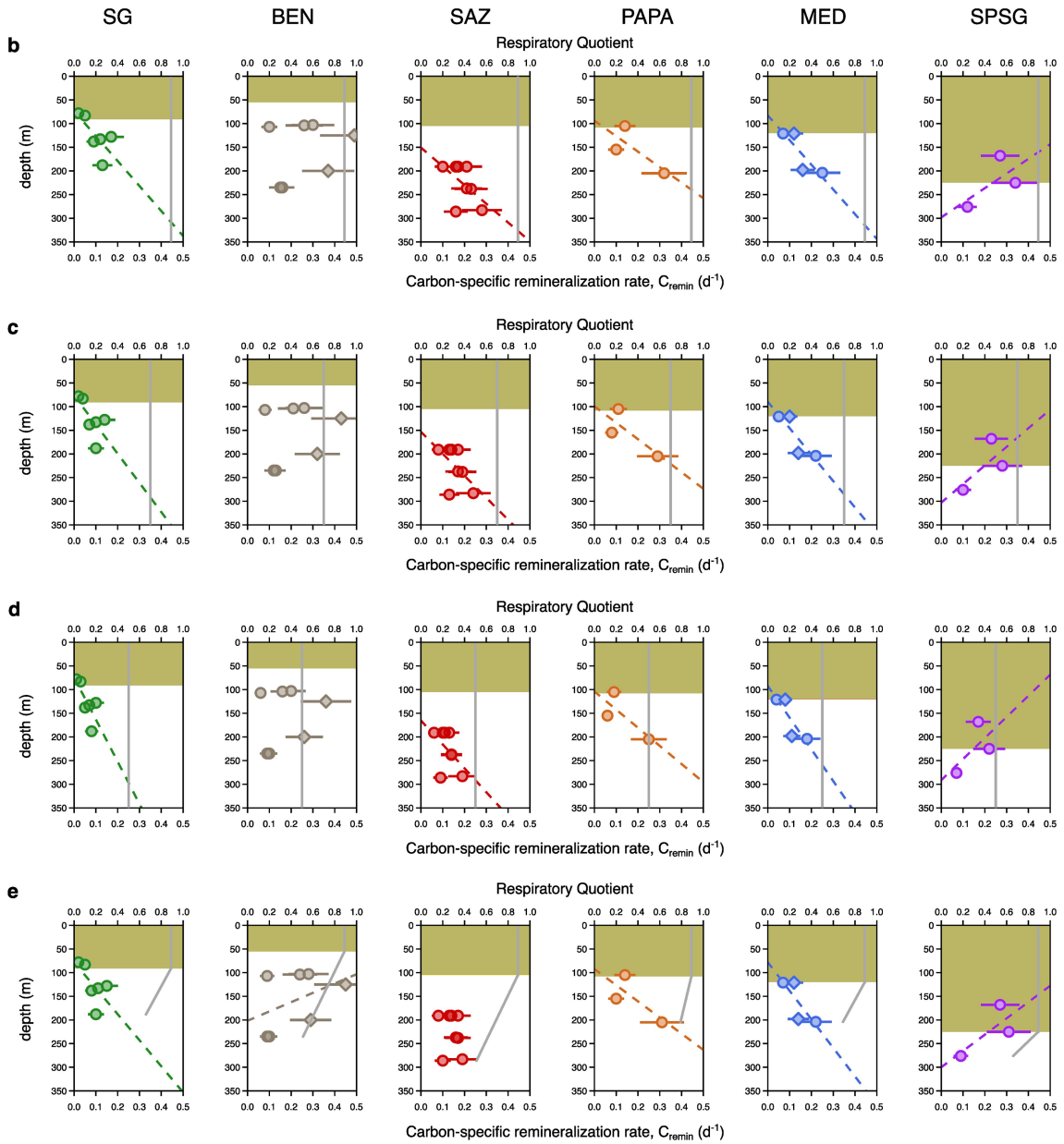


Extended Data Fig. 2 | Functioning of the C-RESPIRE particle interceptor/incubator. (called RESPIRE in Boyd et al.⁹ but referred to C-RESPIRE here to distinguish it from the TM-RESPIRE (see ref. 20)). This figure presents the functioning of the C-RESPIRE particle interceptor/incubator as a conceptual time-series of particle interception (a-c) and rapid transfer of particles (rotating indented solid sphere every 10 min illustrated by the green arrow) into an inner chamber housing an oxygen optode that records dissolved oxygen (DO) every 5 min (denoted in each panel by change from grey to yellow background). Prior to deployment, the inner chamber is filled with <0.2-µm filtered seawater collected at the deployment depth. Panels d-f illustrate the incubation phase

after the periodically-rotating sphere is pre-programmed to halt and the optode tracks the decrease in DO over time. POC remaining at the end of the multi-day incubation is recovered (then analysed) from the inner chamber after first siphoning off all water and particles overlying the sphere within the C-RESPIRE. The exclusion of zooplankton results in the intercepted particles only being degraded by MR during the incubation. Given the likelihood of microbial degradation becoming substrate limited (see Extended Data Fig. 1), this strongly suggests that the residual POC flux can be considered as an indirect measure of the imprint of zooplankton particle transformation processes (see Fig. 1).

a

	RQ = 0.89 *	RQ = 0.70 †	RQ = 0.50 ‡	Depth-varying RQ §
Site	MR contribution to the cumulative POC flux attenuation [%]			
SG	9	7	5	7
BEN	27	23	17	25
SAZ	20	17	13	16
PAPA	27	22	17	27
MED	35	29	23	32
SPSG	25	21	16	25
Range	9 – 35	7 – 29	5 – 23	7 – 32

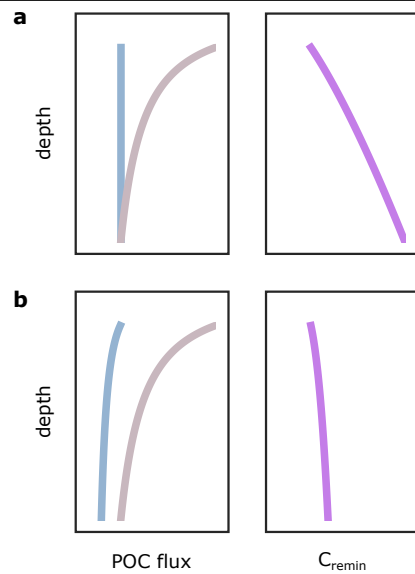


Extended Data Fig. 3 | See next page for caption.

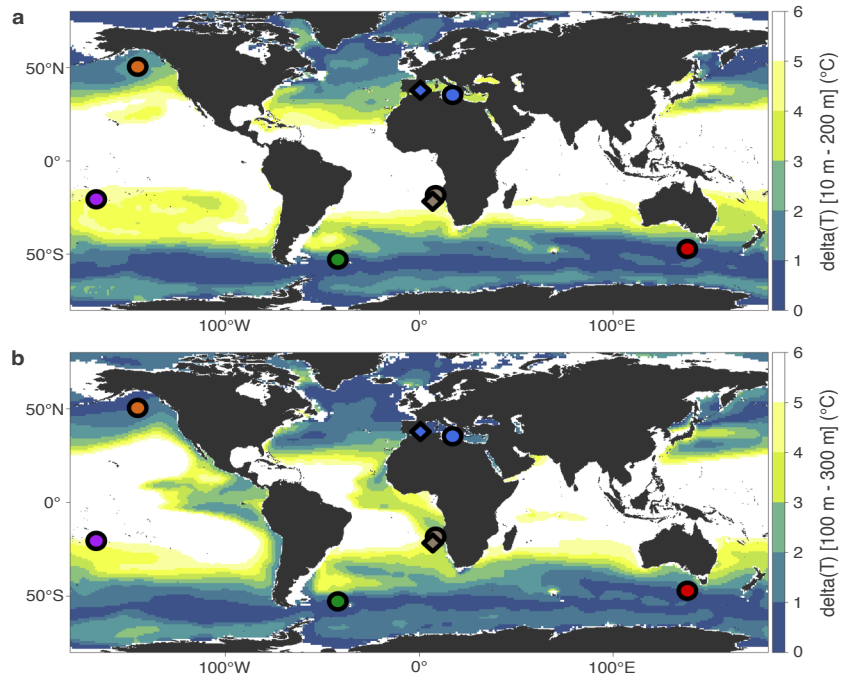
Article

Extended Data Fig. 3 | Investigation of the role of the respiratory quotient (RQ) in influencing the magnitude and vertical patterns of the microbial remineralisation rate. (a) Site-specific median contribution of MR to the cumulative POC flux attenuation obtained using different RQ values (see Methods). * RQ value for a substrate similar to the average composition of planktonic material⁴⁴. † RQ value broadly representative of plankton-based particles⁴⁵ and mesopelagic conditions⁸⁵. ‡ Theoretical minimum RQ value (for methane oxidation⁴⁶). § Depth-varying RQ parameterized using apparent RQ values measured during onboard incubations of sinking particles collected at 180–280 m depth in the Subantarctic and Polar Front zones (see Methods).

Carbon-specific remineralisation rate (C_{remin}) as a function of depth obtained using a RQ of (b) 0.89 (for direct sinking of individual phytoplankton cells⁴⁴), (c) 0.70 (for planktonic based particles such as marine snow⁴⁵), (d) 0.50 (i.e., the theoretical minimum for methane oxidation⁴⁶), and (e) depth-varying aRQ values (see Methods). Grey lines represent the vertical distribution of the RQ values. Yellow-shaded areas represent the primary production zone. Dashed lines represent the best fit of the linear model. Error bars were derived using uncertainty propagation laws (Methods). SG: South Georgia, BEN: Benguela upwelling, SAZ: Subantarctic Zone, PAPA: NE subarctic Pacific, MED: Mediterranean Sea, SPSPG: South Pacific Subtropical Gyre.



Extended Data Fig. 4 | Influence of trends in the profiles for MR and cumulative POC fluxes on the profile shape of the derived metric C_{remin} . Cumulative POC flux (in brown) follows a power-law decrease, while the microbially-mediated contribution to POC flux attenuation (MR) (in blue) is either constant (panel a) or decreases (panel b) with depth, but at a lower rate than the cumulative flux (Fig. 2). The resulting C-specific remineralisation rate (C_{remin} ; in purple), derived from these two components of the POC flux, increases with depth in both scenarios.



Extended Data Fig. 5 | Patterns in the vertical temperature gradient across the global ocean. Temperature gradient (ΔT) in $^{\circ}\text{C}$ over the 10–200 m (a) and 100–300 m (b) depth ranges. Data were obtained from the NOAA World

Ocean Atlas climatology (2005–2017). Colored symbols represent the locations of the C-RESPIRE deployments (same color code as in Fig. 1c) which straddle low and high temperature gradient end-members.

Extended Data Table 1 | Prior investigations of latitudinal trends in *b* values along with explanations of their controlling factors

	<i>b</i> value patterns				
	Approaches	Spatial coverage	Low latitudes	Mid/high latitudes	Controls
Henson et al. [ref. ¹⁰]	Satellite data-derived algorithms	Global ocean	Low	High	Ecosystem structure and recycling in surface
Guidi et al. [ref. ⁸]	UVP imaging and field POC flux data	Global ocean	Low	High	Phytoplankton community structure
Marsay et al. [ref. ⁷]	Sediment traps at multiple depths	Mid-high latitude and (sub)tropical sites	High	Low	Temperature
Weber et al. [ref. ¹³]	PO ₄ used as a tracer of remineralisation in an ocean circulation model	Global ocean	High	Low	Phytoplankton community structure
Cram et al. [ref. ¹⁴]	Model optimized to reproduce <i>b</i> value pattern from Weber et al. [ref. ¹³]	Global ocean	High	Low	Temperature and particle size distribution

Opposing trends for *b* values from Martin curves are evident, as are the proposed differences in the controlling factors. Note, the *b* value reflects wide-ranging particle attenuation processes involving both zooplankton and particle-attached microbes.

Extended Data Table 2 | Overview of the deployments, physico-chemical conditions, and respiration rates measured at the 6 study sites

site	cruise	deployment ID	date	latitude	longitude	depth	collection	incubation	temperature *	<i>in situ</i> O ₂ †	pre-incubation O ₂	ΔO ₂ ‡	respiration rate §		
				[°N]	[°E]				[m]	[d]	[d]	[°C]	[μmol L ⁻¹]	[μmol L ⁻¹]	[μmol O ₂]
SG	COMICS 1	P3A	18/11/2017	-52.69	-40.18	78	1.2	1.3	1.78 (0.18)	363.4	355.6	16.6	11.68 (0.08)	0.98	<0.0001
SG	COMICS 1	P3A	18/11/2017	-52.69	-40.18	128	1.2	1.3	0.84 (0.05)	343.7	302.4	40.3	30.50 (0.32)	0.96	<0.0001
SG	COMICS 1	P3B	30/11/2017	-52.71	-40.08	83	0.9	1.4	1.51 (0.10)	353.6	350.6	17.1	10.62 (0.05)	0.99	<0.0001
SG	COMICS 1	P3B	30/11/2017	-52.71	-40.08	133	0.9	1.4	0.71 (0.16)	330.2	327.6	21.8	14.69 (0.11)	0.98	<0.0001
SG	COMICS 1	P3C	11/12/2017	-52.73	-40.39	138	1.5	0.8	0.79 (0.02)	294.7	283.6	14.5	20.58 (0.10)	1.00	<0.0001
SG	COMICS 1	P3C	11/12/2017	-52.73	-40.39	188	1.5	0.8	1.70 (0.04)	235.0	229.8	23.7	36.19 (0.63)	0.93	<0.0001
BEN	COMICS 2	BS1	26/05/2018	-21.56	9.43	125	0.9	1.1	16.17 (0.18)	219.8	213.9	109.8	52.63 (0.09)	1.00	<0.0001
BEN	COMICS 2	BS1	26/05/2018	-21.56	9.43	200	1.7	1.1	13.38 (0.18)	153.4	133.7	31.6	28.51 (0.34)	0.96	<0.0001
BEN	COMICS 2	BN2	09/06/2018	-18.30	10.95	107	1.5	1.1	13.92 (0.14)	118.30	113.5	51.6	45.52 (0.38)	0.98	<0.0001
BEN	COMICS 2	BN31	15/06/2018	-18.03	11.01	104	1.2	1.1	13.80 (0.17)	126.90	93.4	35.1	46.41 (0.25)	0.98	<0.0001
BEN	COMICS 2	BN31	15/06/2018	-18.03	11.01	235	1.3	1.1	10.94 (0.21)	76.30	44.6	13.1	13.47 (0.26)	0.93	<0.0001
BEN	COMICS 2	BN32	18/06/2018	-18.03	10.99	103	1.2	1.1	13.78 (0.16)	120.80	112.7	39.1	31.31 (0.21)	0.99	<0.0001
BEN	COMICS 2	BN32	18/06/2018	-18.03	10.99	235	1.2	1.1	10.96 (0.14)	50.4	53.6	12.0	8.31 (0.19)	0.85	<0.0001
SAZ	IN2019_V02	RES_08	16/03/2019	-47.00	142.76	191	1.5	1.7	9.49 (0.07)	267.7	264.8	20.2	11.76 (0.02)	1.00	<0.0001
SAZ	IN2019_V02	RES_09	21/03/2019	-46.88	142.02	191	1.5	1.0	10.01 (0.26)	264.5	257.6	4.8	4.21 (0.05)	0.97	<0.0001
SAZ	IN2019_V02	RES_10	27/03/2019	-46.99	142.24	191	1.5	1.3	9.34 (0.13)	272.0	270.5	13.4	9.38 (0.06)	0.99	<0.0001
SAZ	IN2019_V02	RES_10	27/03/2019	-46.99	142.24	237	1.5	1.3	9.20 (0.20)	273.7	271.8	9.9	7.50 (0.05)	0.98	<0.0001
SAZ	IN2019_V02	RES_10	27/03/2019	-46.99	142.24	283	1.5	1.3	9.14 (0.19)	273.3	236.0	35.3	22.16 (0.22)	0.97	<0.0001
SAZ	IN2019_V02	RES_11	30/03/2019	-46.87	142.20	191	1	0.9	9.18 (0.12)	272.2	273.1	3.7	5.67 (0.07)	0.97	<0.0001
SAZ	IN2019_V02	RES_11	30/03/2019	-46.87	142.20	238	1	0.9	9.13 (0.20)	273.5	272.4	6.3	10.38 (0.07)	0.99	<0.0001
SAZ	IN2019_V02	RES_11	30/03/2019	-46.87	142.20	286	1	0.9	9.13 (0.26)	273.2	273.3	5.1	5.27 (0.05)	0.98	<0.0001
PAPA	EXPORTS NP	EPOCH3	31/08/2018	50.58	-144.86	105	1.0	2.0	5.21 (0.08)	252.2	217.6	15.6	8.59 (0.04)	0.99	<0.0001
PAPA	EXPORTS NP	EPOCH3	31/08/2018	50.58	-144.86	155	1.0	2.0	4.80 (0.08)	164.2	161.8	9.3	4.37 (0.01)	0.99	<0.0001
PAPA	EXPORTS NP	EPOCH3	31/08/2018	50.58	-144.86	205	1.0	2.0	4.29 (0.06)	131.5	127.5	21.1	11.41 (0.04)	0.99	<0.0001
MED	PEACETIME	ION	24/05/2017	35.48	19.80	121	3.0	1.7	15.86 (0.02)	224.9	225.7	18.4	15.58 (0.07)	0.99	<0.0001
MED	PEACETIME	ION	24/05/2017	35.48	19.80	204	3.0	1.7	15.47 (0.06)	214.1	220.4	16.4	10.30 (0.01)	0.99	<0.0001
MED	PEACETIME	ALG	02/06/2017	37.95	2.90	121	3.0	2.4	14.20 (0.03)	208.0	191.9	64.3	30.39 (0.07)	1.00	<0.0001
MED	PEACETIME	ALG	02/06/2017	37.95	2.90	198	3.0	2.4	13.60 (0.04)	189.8	185.4	25.6	8.68 (0.06)	0.96	<0.0001
SPSG	TONGA	ST08	18/11/2019	-20.38	-166.46	168	2.1	1	22.67 (0.12)	191.6	182.4	9.3	8.91 (0.15)	0.93	<0.0001
SPSG	TONGA	ST08	18/11/2019	-20.38	-166.46	225	2.1	1	20.38 (0.19)	185.4	180.1	7.4	8.90 (0.09)	0.98	<0.0001
SPSG	TONGA	ST08	18/11/2019	-20.38	-166.46	276	2.1	1	18.62 (0.19)	188.4	184.8	3.3	6.79 (0.08)	0.97	<0.0001

Values in parentheses correspond to the standard deviation of the arithmetic mean of the temperature (averaged over the incubation period), and uncertainty of the linear regression coefficient for respiration rate. * Temperature averaged over the incubation period. † Data obtained from CTD cast(s) performed at the mooring line deployment. ‡ Total amount of O₂ consumed during incubation as defined in the Method section. § Rates obtained from the linear part of the slope using ΔO₂max and Δt (see Extended Data Fig. 1, lower right panel).

Extended Data Table 3 | Overview of the phytoplankton communities at the 6 study sites investigated

Site	Regime	Seasonal amplitude of Chla ^{*†}	PPZ-integrated Chla [mg m ⁻²] [‡]	DCM	Dominant size structure	Dominant groups	Proportion of large diatoms
SG	Productive	0.85	120–400	intermittent	micro- [$>20 \mu\text{m}$]	Large diatoms Dinoflagellates [ref. ⁶³]	High
BEN	Productive	0.47	31 (7)	intermittent	nano- [2–20 μm] + micro- [$>20 \mu\text{m}$]	Large diatoms Dinoflagellates ^a	Low
SAZ	HNLC	0.35	22 (4)	intermittent	nano- [2–20 μm]	Haptophytes Small diatoms [ref. ⁶⁹]	Low
PAPA	HNLC	0.22	24 (1)	absent	nano- [2–20 μm]	Haptophytes Small diatoms [ref. ⁷²]	Low
MED	Oligotrophic	0.56	18–21	present	nano- [2–20 μm]	Cyanobacteria Small diatoms ^b	Low
SPSG	Oligotrophic	0.33	13	present	pico- [$<2 \mu\text{m}$]	Cyanobacteria Picoeukaryotes ^c	Low

These observations were made during the respective campaigns, and/or obtained from published studies for some sites. (Chla = chlorophyll a). * $\text{Log}_{10}(\text{Chla max}) - \text{Log}_{10}(\text{Chla min})$ [ref. 101].
[†] Chla climatologies (2002–2023) obtained from MODIS AQUA (4 km resolution). [‡] Range or average (and standard deviation) of Chla inventories measured during the respective field campaigns.
^a Barlow, R. et al. Environmental influence on phytoplankton communities in the northern Benguela ecosystem. *Afr. J. Mar. Sci.* **40**, 355–370; 2018. ^b Marañón, E. et al. Deep maxima of phytoplankton biomass, primary production and bacterial production in the Mediterranean Sea. *Biogeosciences* **18**, 1749–1767; 2021. ^c Bock, N., Van Wambeke, F., Dion, M. & Duhamel, S. Microbial community structure in the western tropical South Pacific. *Biogeosciences* **15**, 3909–3925; 2018.

Extended Data Table 4 | Dissolved organic carbon (DOC) accumulation rates during incubation

	Lat. [°N]	Lon. [°E]	depth [m]	DOC accumulation [mmol m ⁻² d ⁻¹]
SPSG	-20.4	-166.5	168	0.07 (0.01)
SPSG	-20.4	-166.5	225	0.07 (0.01)
SPSG	-20.4	-166.5	276	0.04 (0.00)
TONGA V2	-19.4	-175.1	166	0.12 (0.01)
TONGA V2	-19.4	-175.1	225	-0.04 (0.0)
TONGA V2	-19.4	-175.1	276	0.08 (0.01)

Accumulation rates were obtained by comparing pre- and post-incubation DOC concentrations measured at SPSPG and TONGA V2. Uncertainties of DOC accumulation (values in parentheses) were obtained by propagating the errors in pre- and post-incubation concentrations. The TONGA V2 site is impacted by shallow hydrothermal activity⁷, and hence not included in this study. Low accumulation rates of DOC within the inner chamber of the C-RESPIRE, representing on average $21 \pm 16\%$ of MR, supports the assumption of a close coupling between solubilisation and microbial respiration within the C-RESPIRE.

Extended Data Table 5 | Apparent RQ values

Site	Latitude (°S)	Longitude (°E)	Z_{PPZ} (m)	Depth (m)	apparent RQ	
					mean	SE
SAZ	47.1	141.4	142	181	0.87	0.06
				230	0.75	0.13
				274	0.84	0.12
PF1	55.9	139.4	122	189	0.77	0.07
				237	0.55	0.07
				283	0.39	0.02
PF2	58.0	141.3	128	191	0.88	0.08
				239	0.58	0.07
				284	0.54	0.12

Apparent RQ values ($aRQ = \Delta DIC / -\Delta O_2$) obtained from onboard incubations of fresh sinking particles collected in the mesopelagic at 3 different sites and depths using surface-tethered particle interceptor traps deployed in the Subantarctic Zone (SAZ) and Polar Front zone (PF1 and PF2) (see Methods).